

Phenotypic miRNA Screen Identifies miR-26b to Promote the Growth and Survival of Endothelial Cells

Andrea Martello,¹ David Mellis,¹ Marco Meloni,¹ Alison Howarth,² Daniel Ebner,² Andrea Caporali,¹ and Ayman Al Haj Zen^{2,3}

¹British Heart Foundation Centre for Cardiovascular Science, QMRI, University of Edinburgh, Edinburgh EH16 4TJ, UK; ²Target Discovery Institute, Nuffield Department of Medicine, University of Oxford, Oxford OX3 7FZ, UK; ³British Heart Foundation Centre of Research Excellence, Division of Cardiovascular Medicine, Radcliffe Department of Medicine, University of Oxford, Oxford OX3 9DU, UK

Endothelial cell (EC) proliferation is a crucial event in physiological and pathological angiogenesis. MicroRNAs (miRNAs) have emerged as important modulators of the angiogenic switch. Here we conducted high-content screening of a human miRNA mimic library to identify novel regulators of EC growth systematically. Several miRNAs were nominated that enhanced or inhibited EC growth. Of these, we focused on miR-26b, which is a conserved candidate and expressed in multiple human EC types. miR-26b overexpression enhanced EC proliferation, migration, and tube formation, while inhibition of miR-26b suppressed the proliferative and angiogenic capacity of ECs. A combinatory functional small interfering RNA (siRNA) screening of 48 predicted gene targets revealed that miR-26b enhanced EC growth and survival through inhibiting PTEN expression. Local administration of miR-26b mimics promoted the growth of new microvessels in the Matrigel plug model. In the mouse model of hindlimb ischemia, miR-26b was found to be downregulated in endothelium in the first week following ischemia, and local overexpression of miR-26b improved the survival of capillaries and muscle fibers in ischemic muscles. Our findings suggest that miR-26b enhances EC proliferation, survival, and angiogenesis. miR-26b is a potential target for developing novel pro-angiogenic therapeutics in ischemic disease.

INTRODUCTION

Blood vessels remain mostly quiescent throughout adult life. However, in response to injury or pathological conditions, they maintain the capacity to rapidly form a new vascular network from pre-existing vessels in a complex process called angiogenesis.¹ During sprouting angiogenesis, while tip cells are highly migratory endothelial cells (ECs) that guide the new sprout toward pro-angiogenic gradients, neighboring stalk cells elongate the new sprout by their highly proliferative capacity.² EC proliferation is also involved in other types of post-natal angiogenesis, such as enlargement of pre-existing capillaries and bridging or intussusception of enlarged vessels to form smaller daughter vessels.³

Both the survival and growth of the pre-existing capillary network have been demonstrated to be major determinant factors for the formation of a functional vascular network and re-establishing the tissue reperfusion in response to ischemic injury.^{4,5} For instance, vascular endothelial growth factor (VEGF) and other vascular growth factors, such as fibroblast growth factor (FGF), bind to their receptors on ECs and stimulate the downstream PI3K-AKT1-mTOR pathway, which is essential for EC proliferation and survival.⁶⁻¹⁰ Impairment of EC growth and survival pathways causes a deficiency in post-ischemic angiogenesis.^{11,12} Patients with limb ischemia have a lower capillary density of skeletal muscles, and that is related to the functional impairment capacity,¹³ indicating the presence of an insufficient adaptive mechanism of angiogenesis to compensate the lack of blood supply in ischemic muscles. Thereby, the induction of angiogenesis in ischemic vascular disease would be beneficial, including enhancing EC growth, which is a hallmark of angiogenesis.

MicroRNAs (miRNAs) are single-stranded RNAs that target mRNAs with complementary sequences, leading to their transcript destabilization, translational inhibition, or both.^{14,15} Previous reports have demonstrated that the miRNA pathway can be critical for vascular development, post-natal angiogenesis, and pathological angiogenesis.¹⁶⁻¹⁸ Many miRNAs were identified to be essential for angiogenesis and vascular response after injury. For example, it has been reported that miR-221 is required for endothelial tip cell behavior during vascular development.¹⁹ EC-selective miR-15a transgenic overexpression leads to reduced blood vessel formation and local blood flow perfusion in mouse hindlimbs.²⁰ miR-503 caused EC

Received 26 February 2018; accepted 14 August 2018;
<https://doi.org/10.1016/j.omtn.2018.08.006>.

Correspondence: Ayman Al Haj Zen, British Heart Foundation Centre of Research Excellence, Division of Cardiovascular Medicine, Radcliffe Department of Medicine, University of Oxford, Oxford OX3 9DU, UK.

E-mail: ayman.alhajzen@cardiov.ox.ac.uk

Correspondence: Andrea Caporali, British Heart Foundation Centre for Cardiovascular Science, University of Edinburgh, Edinburgh EH16 4TJ, UK.

E-mail: a.caporali@ed.ac.uk



dysfunction and impaired post-ischemic vascular repair.^{21,22} Furthermore, miRNA expression changes have been associated with several vascular diseases.^{23–25}

Phenotypic high-content screening offers a systematic approach exploring a large number of genome-wide libraries of small interfering RNAs (siRNAs) and miRNAs, allowing the unbiased analysis of a high number of cells, at the single-cell level.^{26,27} The use of this approach has been applied successfully for the identification of miRNAs regulating cellular processes involved in cardiovascular physiology and pathology.^{28–30} Here we conducted a comprehensive functional high-content miRNA screening to identify miRNAs triggering EC growth, using an entire human miRNA mimic library, which could be potentially novel targets for therapeutic angiogenesis. We identified miR-26b as an enhancer of EC survival and growth *in vitro* and *in vivo*.

RESULTS

Screening for miRNAs Regulating EC Growth

We conducted a phenotypic high-throughput screening of a human miRNA mimic library for their effect on human umbilical vein EC (HUVEC) growth. The quality of the screen was assessed by measurement of the Z' factor, which resulted in a technical Z' factor of >0.3 per plate and overall Z' factor of 0.3 (Figure S1). The screening results showed 129 miRNAs enhanced EC growth by more than 0.85 log fold change (equivalent to 1.8-fold at linear scale) when compared with the ECs treated with the miRNA controls, and 182 miRNAs reduced the EC growth (log2 fold change <−0.85) (Figure 1A). The screening was performed in duplicate; the replicates showed excellent reproducibility ($r^2 > 0.8$; Figure 1B). Importantly, many of the well-characterized miRNAs regulating cell proliferation and/or angiogenesis, including miR-17, miR-221, and miR-302c, are included in our screening results.

We next concentrated on miRNAs enhancing EC growth. Based on data retrieved from small RNA sequencing datasets (Encyclopedia of DNA Elements [ENCODE]), we found 24 were both evolutionarily conserved and accounted for their expression in four different EC sources: HUVECs, human coronary artery endothelial cells (HCAECs), human aorta endothelial cells (HAECs), and human dermal micro-vascular endothelial cells (HMVECs) (Figures 1C and 1D). Among 24 miRNAs, five miRNAs (miR-32, miR-381, miR-26b, miR-379, and miR-1271) had not previously been reported to regulate EC growth activities and angiogenesis in the literature. miR-26b has the highest expression in ECs compared to the other four hits. Therefore, we chose miR-26b to focus on for validation and mechanistic follow-up studies.

miR-26b Regulates EC Growth, Survival, and Tube Formation

To confirm the effect of miR-26b on EC proliferation, we measured DNA synthesis using an EdU cell proliferation assay. We found that miR-26b significantly enhanced EdU incorporation and mitotic index in HUVECs (Figure 2A). Furthermore, miR-26b exerted a pro-survival effect on ECs under starvation for 24 hr or following expo-

sure to H₂O₂ (Figure 2B). The pro-survival effect of miR-26b on HUVECs was confirmed by the increase of AKT1 phosphorylation level (Figure 2C). The proliferative and pro-survival effects of miR-26b were abolished when it was incubated with dominant-negative inhibition of AKT1 signaling (Figure S2).

Using electric cell-substrate impedance sensing (ECIS), we found that miR-26b overexpression increased EC migration speed (Figure 2D). The overexpression of miR-26b enhanced the EC tube formation and branching morphogenesis in full vascular growth factor media or reduced vascular growth factor media (Figure 2E). Next, we investigated the effect of miR-26b inhibition using anti-miRs on EC growth and tube formation, and we found the anti-miR-26b decreased both VEGF-driven EC growth and tube formation (Figures 2F and 2G). We determined whether the endogenous expression of its family member miR-26a is affected by the miR-26b overexpression or inhibition, and we found that the expression level of miR-26a is not affected by the modulation of miR-26b expression (Figure S3). Our observations reveal that, *in vitro*, miR-26b regulates EC growth, survival, migration, and tube formation.

Identification of miR-26b Gene Target-Mediated EC Growth and Survival

It is important to note that identifying functionally important miRNA targets is crucial for understanding miRNA functions. Bioinformatic analysis of miR-26b targets revealed more than 2,000 predicted gene targets. Consequent functional annotation analysis of predicted target genes revealed enrichment for genes belonging to FGF-, transforming growth factor β (TGF- β)-, p53-, and apoptosis-signaling pathways, which are related to cell growth and survival functions (Figure 3A). Among the genes in these, we focused on 48 gene candidates selected from the top-ranked pathways to study their potential regulation by miR-26b. We applied two phenotypic loss-of-function approaches to prioritize the gene targets using a siRNA screen of 48 gene target candidates. First, to determine which gene target mediates the pro-proliferative effect of miR-26b, siRNA-transfected HUVECs were co-transfected with miR-26b or miR-control mimic. We found that four siRNAs (PTEN, PMAIP1, PCK1, and CREBBP) that prevented miR-26b induced more than two folds of EC growth (Figure 3B). Second, we investigated the siRNA-transfected HUVECs on the survival rate in the presence of H₂O₂ exposure for 24 hr. We identified three genes (PTEN, PPP2R2A, and PMAIP1) that enhance EC survival rate with similar potency compared with miR-26b (Figure 3C).

PMAIP1 (also known as Noxa) and PTEN resulted from the two functional assays, and both negatively regulate cell survival.^{31,32} PPP2R2A was excluded from further analysis because it was not regulated at an mRNA or protein level by miR-26b mimics or anti-miR-26b (Figure S4). To further validate direct miRNA binding in the 3' UTR of PTEN and PMAIP1, we used the luciferase reporter vector system as described before,²¹ in which 3' UTR luciferase plasmids of PTEN and PMAIP1 were co-transfected with miR-26b mimic or its control mimics into HEK293 reporter cells. We were not able to perform luciferase gene reporter assays in ECs because of low

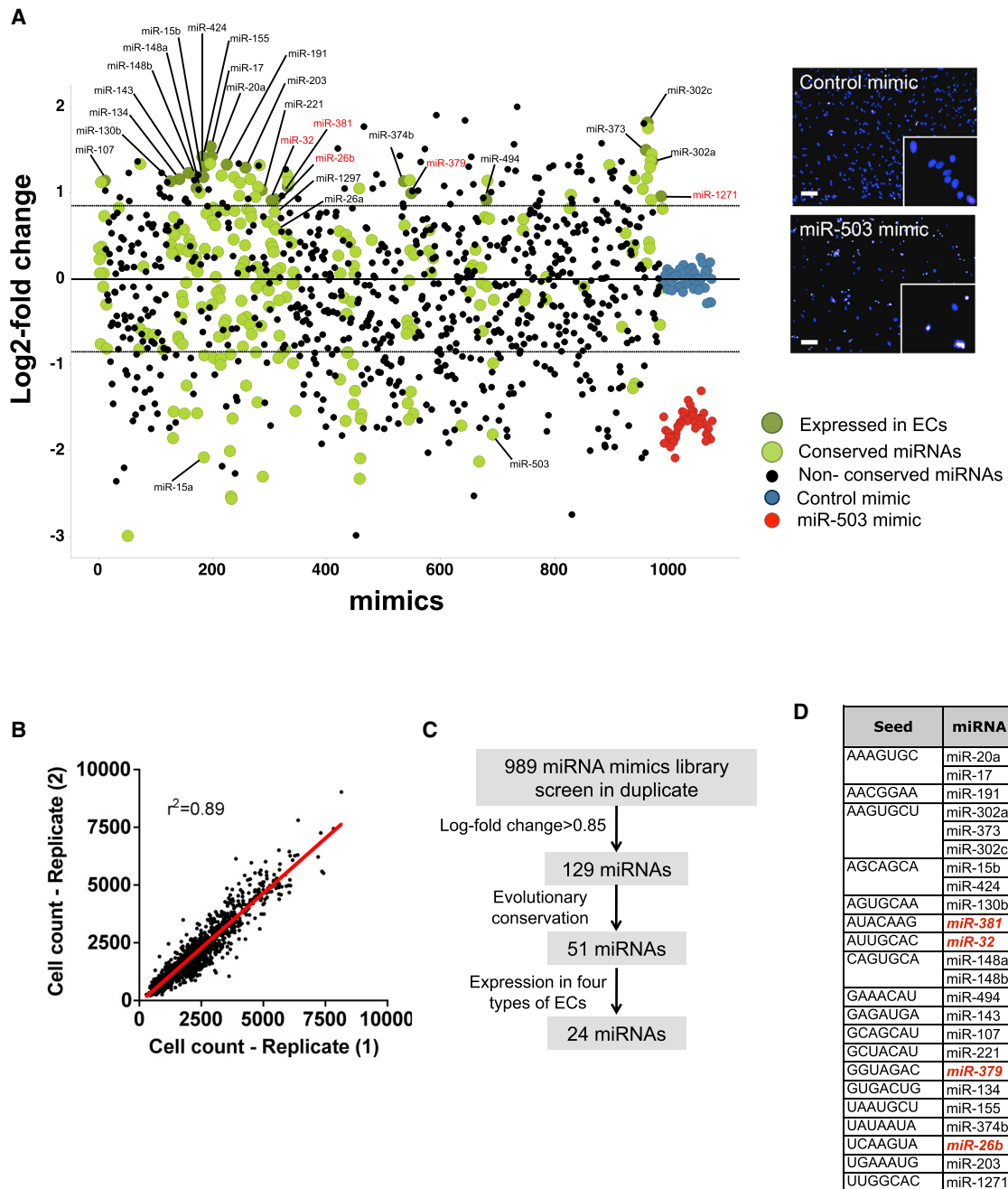


Figure 1. Phenotypic Screen of miRNAs Regulating HUVEC Growth

(A) Left panel: \log_2 (fold change of miR mimics versus control mimics) values of cell count on the y axis is plotted against miR-mimics on the x axis. Non-conserved miRNAs (black), conserved miRNAs (light green), and miRNA enhancers of cell growth that are conserved and expressed in endothelial cells (dark green) are shown. Positive controls, miR-503 mimic, red; negative controls, miR-control mimic, blue; black dashed lines, cutoff \log_2 values in either direction >0.85 or <-0.85 . Right panel: representative images of negative and positive controls from a screen plate. Nuclei were stained with DAPI (blue). Scale bar, 100 μm . (B) Correlation of screen plate replicates for the raw data of cell count parameter ($r^2 = 0.89$). (C) Schematic describing the filtering and selection process of hit enhancers. (D) The selected hit enhancers are listed with their seed region. These miRNAs are expressed among four different EC types: HUVECs, human coronary artery endothelial cells (HCAECs), human aorta endothelial cells (HAECs), and human dermal micro-vascular endothelial cells (HMVECs). miRNAs that have not previously been studied in the context of angiogenesis are in red.

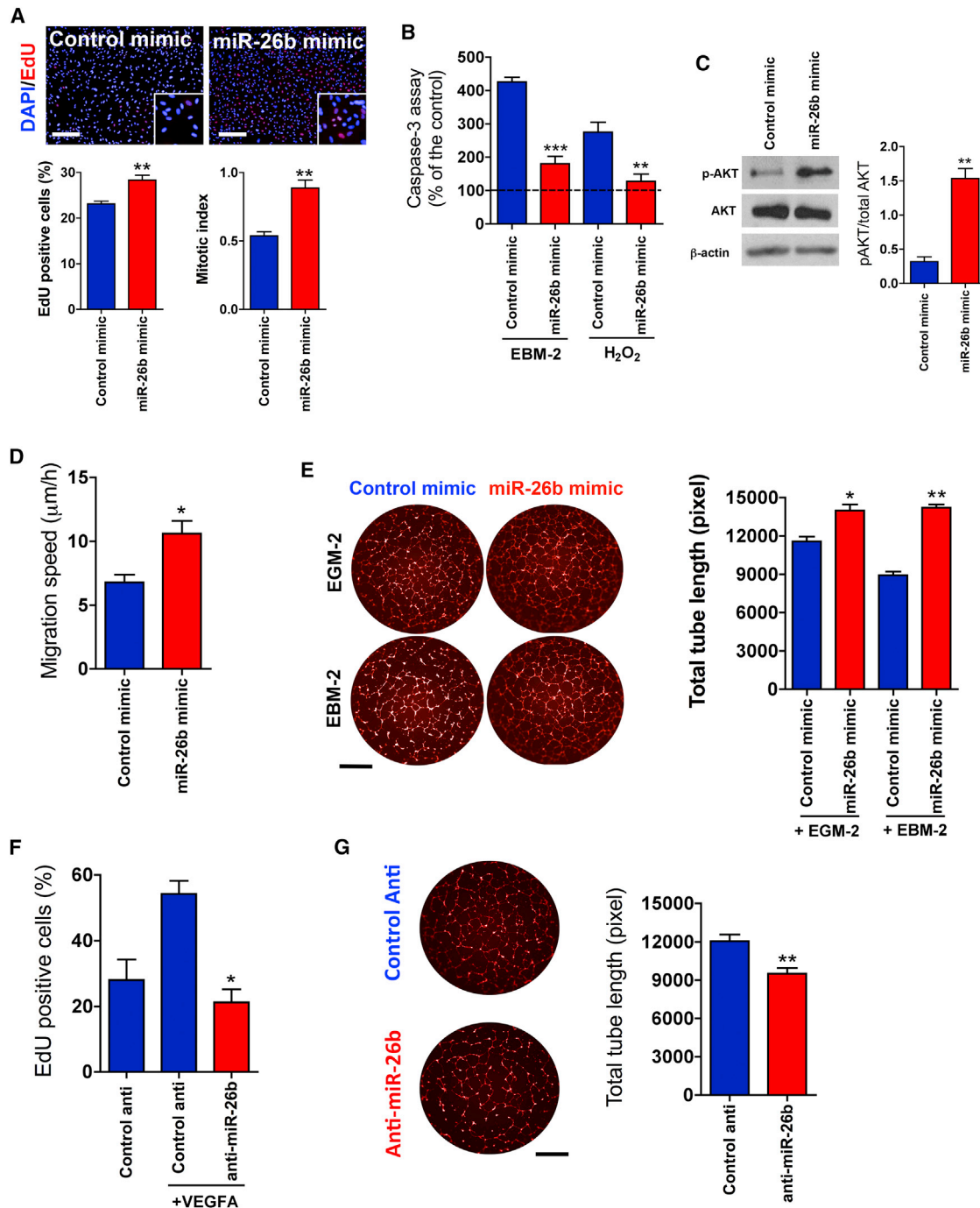


Figure 2. miR-26b Regulates EC Growth, Survival, Migration, and Tube Formation

(A) Upper panel: representative images showing the effect of miR-26b mimics on cell number and DNA synthesis in HUVECs. Cells were fixed 72 hr after mimic transfection. Cells were stained for EdU (green) and DAPI (blue). Scale bars, 200 μ m. Lower panel: quantitative data for the proportion of EdU-positive nuclei and mitotic cells to total cell number are shown. Mitotic cells are identified by their high content of EdU and DAPI staining. Mitotic index is the ratio between the number of cells in mitosis and the total number of cells. Error bars are mean \pm SEM; ** p < 0.01 compared to miR-control mimic (n = 6 replicates, unpaired t test). (B) Effect of miR-26b mimics on apoptosis induced by starvation (EBM-2) or H₂O₂ (500 μ M). H₂O₂ was added after 48 hr of transfection for an additional 24 hr. Measured caspase-3 activity is normalized to controls and is expressed as mean \pm SEM; n = 4 per condition; one-way ANOVA followed by Bonferroni post hoc test, * p < 0.01 and ** p < 0.001 compared to miR-control mimics. (C) Immunoblotting for phospho-AKT (p-AKT^{S473}) and total AKT1 (65 kDa) detection in HUVECs after 72 hr of miR-26b mimic or miR-control mimic transfection. β -actin was detected as a loading control. (D) Effect of miR-26b mimic on HUVEC migration speed measured for 8 hr by electric cell-substrate impedance sensing. The assay was

(legend continued on next page)

transfection efficacy. Luciferase activity was significantly lowered when miR-26b was transfected compared with control mimic treatment, whereas mutation of the binding sites restored it (Figure 3D). We validated that miR-26b mimics downregulated the mRNA expression of the two target gene candidates, whereas anti-miR-26b increased their expression (Figure 3E). Western blot analysis demonstrated that only PTEN is regulated at a protein level at 72 hr after transfection with miR-26b mimic or anti-miR-26b (Figure 3F), whereas PMAIP1 is downregulated by miR-26b mimic only at 16 hr after transfection and accumulated at the same control levels after 48 hr (Figure S5). Thus, we found that PTEN in ECs is the most suitable target among the selected genes.

miR-26b Promotes *In Vivo* Microvascular Growth

To investigate whether miR-26b has pro-angiogenic properties *in vivo*, miR-26b mimic and miR-control mimic were incorporated in the Matrigel and injected subcutaneously into the mice. After 12 days, mimics regulated miR-26b expression in the plugs (Figure 4A), resulting in the opposite expression of its identified target gene PTEN at protein and mRNA levels (Figures 4B and 4C). Matrigel plugs mixed with miR-26b mimic exhibited more neovascularization, characterized by the increase of CD31-stained area, than those mixed with control mimic (Figure 4D). The quantification of mature microvessels, determined on the basis of pericyte or smooth muscle cell-covered endothelium (vascular structures that are double positive for α -smooth muscle [SM] actin and CD31), confirmed that miR-26b mimic enhances the induction of mature vasculature (Figure 4E). This suggests that, *in vivo*, forced overexpression of miR-26b enhances the microvascular growth and mature neovascularization.

miR-26b Increases *In Vivo* EC Survival following Acute Ischemia

To assess the endogenous expression of miR-26b level in response to ischemic insult, ECs were isolated from mouse adductor muscles at 3, 7, and 14 days following the induction of limb ischemia. The EC population was sorted based on the high expression of CD31 and the lack of CD45 expression. EC purity was confirmed by the co-expression of other constitutive EC markers, such as CD144 (VE-cadherin) and CD105 (endoglin) (Figure S6). The expression level of miR-26b in isolated ECs significantly decreased at 3 and 7 days post-ischemia compared with sham-operated controls (Figure 5A). Of note, the expression level of miR-26b after ischemia was altered only in the endothelium and it was not in the whole of ischemic muscle fraction (Figure 5B).

Next, we evaluated whether administration of miR-26b mimics would improve EC survival following ischemic injury. Recently the efficacy of different lipid formulations in delivering miRNA mimics has been confirmed in a mouse model of ischemia.³³ Mice were subjected to hindlimb ischemia and followed by local administration of miR-26b or miR-control mimics, complexed with a lipid transfection reagent. At day 3 after injection, we first measured the expression levels of the injected miR-26b mimic and its target PTEN in the isolated ECs from adductor muscle and in total adductor muscle. We detected a significant increase in the levels of miR-26b in both ECs and total muscle (Figure 6A). This was associated with a significant decrease in the expression level of PTEN (Figure 6B), indicative of effective transfection and sustained activity of forced expressed miR-26b.

Histological examination of muscle cross-sections revealed less necrotic areas in the ischemic muscles treated with miR-26b mimic compared to control (Figure 6C). The pro-survival effect of miR-26b on ECs and myocytes was confirmed by terminal deoxynucleotidyl transferase dUTP nick end labeling (TUNEL) staining. We found that the overexpression of miR-26b resulted in a significant reduction of apoptosis in both ECs and myocytes (Figure 6D). We assessed the effect of miR-26b overexpression on the survival of native microvasculature network structure following ischemia injury. Confocal three-dimensional (3D) imaging exhibited a better preservation of native microvasculature network integrity in the necrotic area of ischemic adductor muscles treated with miR-26b mimic compared to the controls (Figure 7).

Next, we tested whether the local overexpression of miR-26b mimic could affect the remodeling of collateral arterioles in the ischemic adductor muscles, and we found no difference in the total area of α -SM actin-positive collateral vessels between miR-26b mimic-treated adductor muscle and the controls after 3 days of ischemia injury (Figure S7A). Moreover, both the miR-26b mimic-treated group and control mimic-treated group showed no difference in foot perfusion recovery during the 3 days following femoral excision (Figure S7B). Collectively, these results show that local overexpression of miR-26b enhances the survival of native microvasculature network following ischemia injury, which is associated with less muscle fiber necrosis.

DISCUSSION

Cell proliferation is stimulated only in vascular ECs needed for the growth of new blood vessels or vascular repair after injury. Using a

performed 72 hr after mimic transfection. Error bars are mean \pm SEM; * p = 0.02 compared to miR-control mimic (n = 4 replicates, unpaired t test). (E) Left: representative images showing effect of miR-26b mimics on EC tube formation with vascular growth factor media (EGM-2) or without growth factor media (EBM-2). Scale bar, 1 mm. The assay was performed 72 hr after mimic transfection. Tubes were fixed after 8 hr and stained with phalloidin alexa 568. Right: total tube length (pixels) is expressed as mean \pm SEM; n = 5 per condition; one-way ANOVA followed by Bonferroni post hoc test, * p < 0.01 and ** p < 0.001 compared to miR-control mimics. (F) Effect of anti-miR-26b on DNA synthesis in HUVECs activated by VEGFA (10 ng/mL) during the experiment. Cells were fixed 72 hr after mimic transfection. EdU-positive cell percentage is expressed as mean \pm SEM; n = 4 per condition; one-way ANOVA followed by Bonferroni post hoc test, * p < 0.01 compared to control anti-miR. (G) Effect of anti-miR-26b on EC tube formation. Representative bright-field images of tube formation for HUVECs transfected with anti-miR-26b and control anti. Scale bar, 1 μ m. The assay was performed 72 hr after anti-miR transfection. Tubes were fixed after 8 hr and stained with phalloidin alexa 568. Error bars are mean \pm SEM; ** p < 0.01 compared to control anti-miR (n = 6 replicates, unpaired t test).

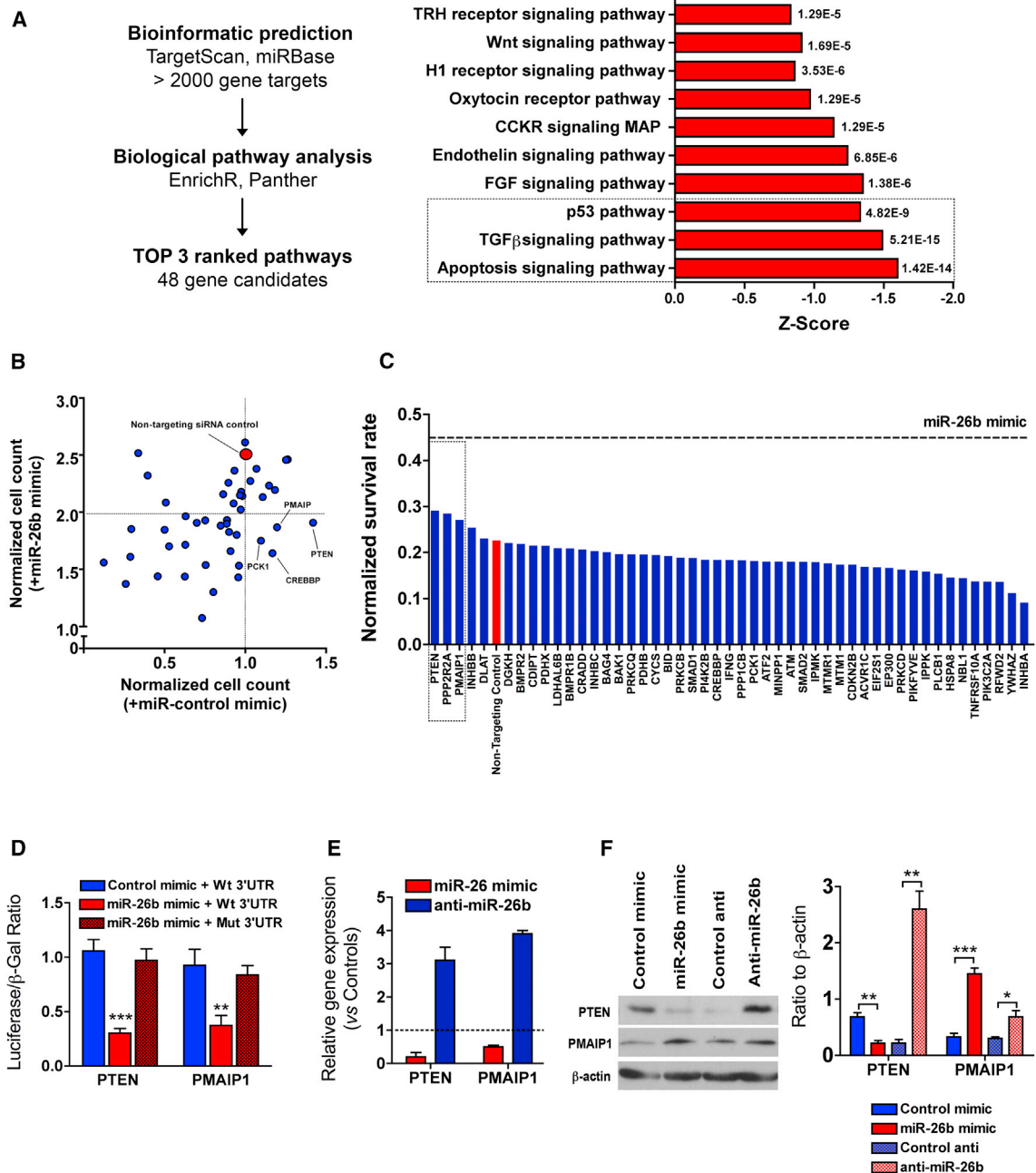


Figure 3. Identification of miR-26b Target Genes

(A) Workflow for miRNA target identification (left panel). Genes were classified into molecular function according to the PANTHER classification system using EnrichR open source. Signaling pathways identified by the PANTHER classification system were plotted based on Z scores within each pathway (right panel). (B) siRNA-transfected HUVECs co-transfected with miR-control or miR-26b mimics. Cell count was captured 72 hr later. Cell count was normalized to non-targeting siRNA control-/miR-control mimic-transfected cells. Horizontal dashed line shows the cutoff value <2-fold for target genes abolishing the effect of pro-proliferative of miR-26b mimic. (C) siRNA-transfected HUVECs were incubated without or with a high dose of H_2O_2 (500 μM) for 24 hr. Horizontal dashed line shows the survival rate level of miR-26b mimic-transfected cells. Non-targeting siRNA control, red. (D) Luciferase gene reporter assays in HEK293 cells confirmed miR-26b binding to wild-type (WT) 3' UTR or mutated (mut) 3' UTR of PTEN and PMAIP1. Data are shown as the mean \pm SEM of 6 independent experiments; ** $p < 0.01$ and *** $p < 0.001$ versus miR-control mimic. Two-way ANOVA followed by Bonferroni post hoc test. (E) HUVECs were transfected with miR-26b mimic, anti-miR-26b, miR-control mimic, or anti-miR-control. At 3 days post-transfection, RNA was extracted and the levels of PTEN and PMAIP1 were determined by qRT-PCR. Values were normalized to S18 and then to the controls (mimic or anti-miR). Data are shown as the mean \pm SEM of 4 independent experiments (* $p < 0.01$). (F) Cells were lysed and the expression of PTEN and PMAIP1 were analyzed by immunoblotting. β -actin was detected as a loading control.

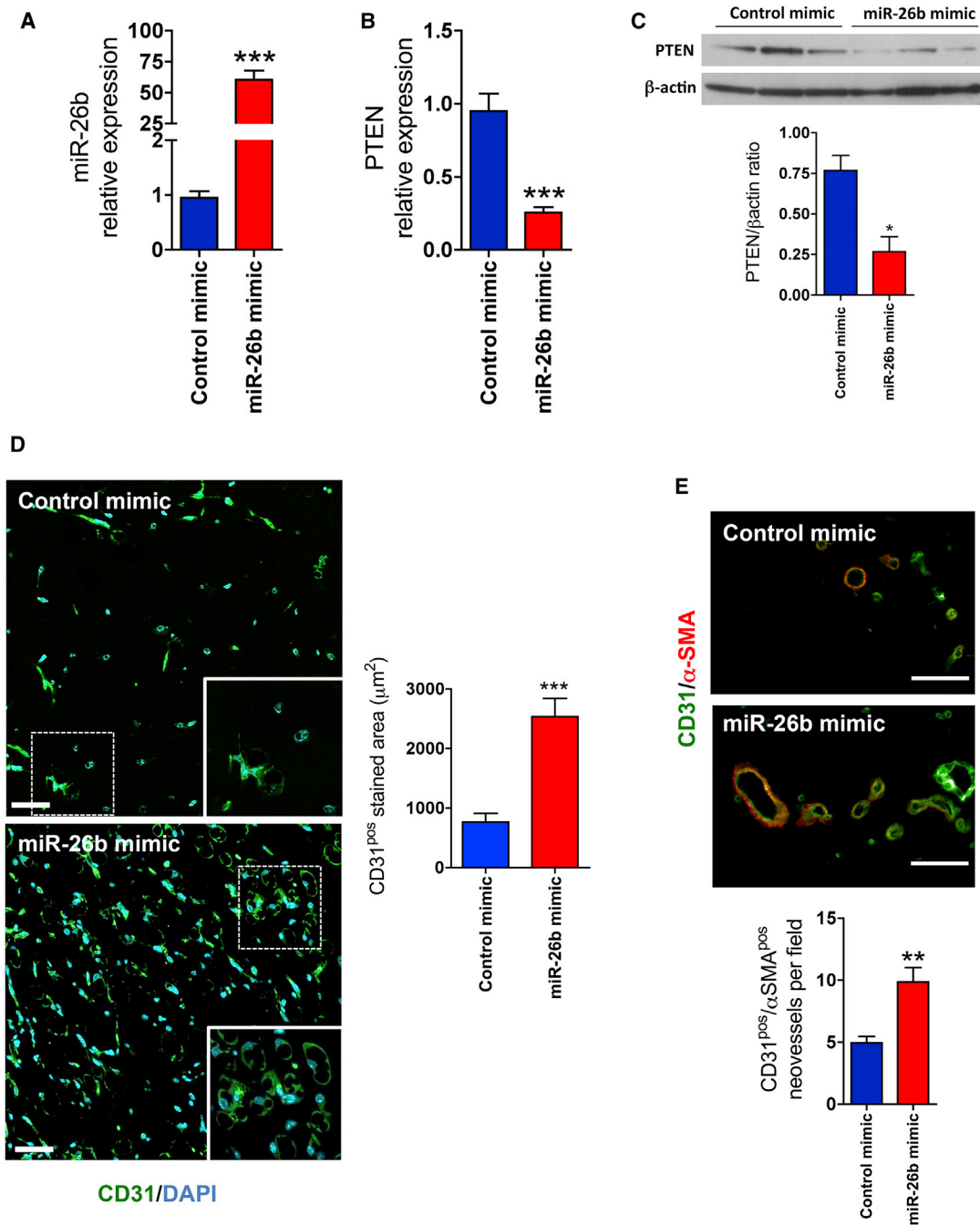


Figure 4. miR-26b Promotes Microvascular Growth *In Vivo*

(A and B) The expression of (A) miR-26b and (B) PTEN in Matrigel plug mixed with miR-26b mimic and control mimic after 12 days. (C) Western blot analysis of PTEN expression in Matrigel plugs. β -actin was detected as a loading control. Lower panel: quantification of western blotting is shown. Error bars are mean \pm SEM; * $p < 0.05$ compared to controls ($n = 3$ animals per group, unpaired t test). (D) Left panels: representative images showing the new microvessels positive for CD31 (green), with the predominant linear structures indicating small vessels and some apparently circular structures indicating larger vessels in the implanted plugs. Scale bars, 50 μ m. Right panel: quantification of the area of CD31 coverage in the Matrigel plugs mixed with miR-26b mimic or control mimic at 12 days after implantation is shown. (E) Upper panel: representative images of Matrigel plugs showing structures double positive for green (CD31) and red (α -SM actin) indicate vessels with mural cell coverage, which are more mature vessels. Scale bar, 25 μ m. Lower panel: quantification of the number of double-positive CD31 and α -SM actin vessels per field in the Matrigel plugs mixed with miR-26b mimic or control mimic at 12 days after implantation is shown. Error bars are mean \pm SEM; ** $p < 0.01$ and *** $p < 0.001$ compared to controls ($n = 6$ animals per group, unpaired t test).

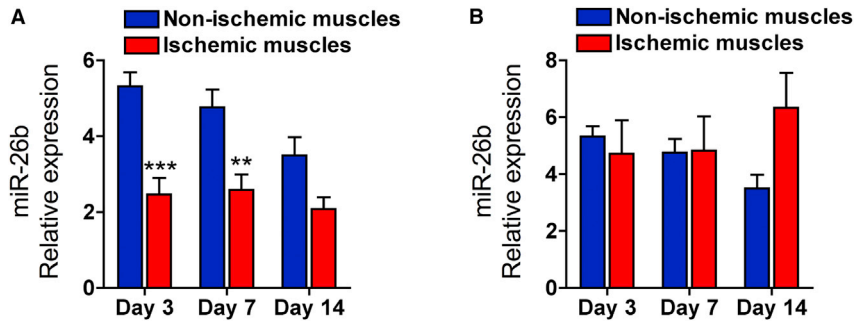


Figure 5. Time Course of Endogenous miR-26b Expression in the Adductor Muscle following Ischemia Injury

(A and B) Expression of miR-26b in (A) endothelial cell (CD31^{pos}/CD45^{neg}) fraction and (B) muscle fraction isolated from the adductor muscles, which were collected at 3, 7, and 14 days after ischemia induction. miR-26b levels were normalized against snRU6 control. Error bars are mean \pm SEM; **p < 0.01 and ***p < 0.001 compared to controls (n = 6 replicates, unpaired t test).

high-throughput screening approach of an miRNA mimic library, we found many miRNAs positively and negatively modulate the EC growth. For instance, miR-17 and miR-221 were identified as enhancers of EC growth. A previous study showed that VEGF-mediated upregulation of miR-17 expression was necessary for *in vitro* EC proliferation and angiogenic sprouting. Furthermore, *in vivo* specific deletion of miR-17 in endothelium has reduced physiological retinal angiogenesis during development and diminished VEGF-induced tumor angiogenesis.³⁴ miR-221 has been shown to be required for endothelial tip cell proliferation and migration. Exogenous miR-221 expression increased bromodeoxyuridine (BrdU) incorporation in cells that contributed to the dorsal longitudinal anastomotic vessels in the zebrafish.¹⁹ Our phenotypic screening revealed that miRNAs, such as miR-15a, miR-24, and miR-503, decreased EC growth significantly. These miRNAs have been previously studied in EC biology, and they demonstrated their deleterious effect on EC proliferation and angiogenesis.^{21,35,36}

miR-26b Is an Enhancer of Endothelial Cell Growth

Among miRNA hits, miR-26b was identified as a novel candidate that enhances EC proliferation and survival in several relevant *in vitro* and *in vivo* models. miR-26b is a member of the miR-26 family, which is localized on chromosome 2. The other members of the family constitute miR-26a-1, localized on chromosome 3, and miR-26a-2, localized on chromosome 12. Their mature products share an identical sequence.³⁷ It only differs from the mature miR-26b sequence by 2 nt. They are predicted to target nearly identical sets of genes. However, it seems that the miR-26a isoform has a different role in EC proliferation and angiogenesis. Indeed, it has been shown that overexpression of miR-26a induced cell-cycle arrest and inhibited the *in vitro* angiogenesis through targeting smad1 3' UTR. The systemic administration of LNA-anti-miR-26a increased angiogenesis, improved heart function following infarction, and decreased infarct size.³⁸ A possible explanation for these discrepancies is that miR-26b levels vary significantly in response to an angiogenic stimulus, suggesting that growth conditions influence miRNA function in cultured cells.

Upon the stimulation of ECs by TNF- α or VEGF, the expression levels of both miR-26a and miR-26b were downregulated distinctively.³⁸ In other primary vascular cells, miR-26a promotes smooth muscle cell

proliferation via the TGF- β -signaling pathway. Conversely, the inhibition of miR-26a enhanced a contractile phenotype of smooth muscles.³⁹ Our findings and those of others show that the actions of miR-26b are not shared by miR-26a, which would be valuable to examine in future vascular studies.

Previous studies have demonstrated that the expression level of miR-26b is reduced in the tissues of many cancers of liver,⁴⁰ breast,⁴¹ and colon.⁴² Functionally, miR-26b exerts a tumor-suppressive role in many types of cancer, and the miR-26b-mediated growth inhibition is achieved through suppression of target genes like OCT4,⁴³ SMAD1, CTGF,⁴⁴ and/or COX2.⁴⁵ In contrast, overexpression of miR-26a in a murine glioma model enhances *de novo* tumor formation.³⁷ These observations raise the possibility that the miR-26 family governs context-specific changes in endothelial behavior depending on cell type or tissue microenvironment. Thus, while miR-26b plays an important pro-proliferative and survival signal during angiogenesis, it may play different roles in cancer cell growth.

Validation of miR-26b Targets

The phenotypic approach can be used for miRNA target identification, recognizing the targets that are relevant for a specific phenotype. This is particularly important because one miRNA can have hundreds of putative targets, but only a few of these might be accountable for the phenotype under investigation. In this study, by combining target prediction- and functional RNAi-screening approaches, we have prioritized two gene target candidates, PTEN and PMAIP1, that could be responsible for the proliferative and survival phenotype induced by miR-26b. Within the 3' UTR region of both mRNA targets, there are potential binding sites for miR-26b, and accordingly, we detected a robust downregulation of mRNA levels of the two target genes.

PMAIP1 has been shown to be a critical mediator of apoptotic signaling, and it functions primarily by inactivating the anti-apoptotic Bcl-2 family protein Mcl-1.⁴⁶ Elevated PMAIP1 levels were detected after transient ischemia experiments *in vivo*, and delivery of PMAIP1 antisense oligonucleotides significantly reduced infarct volumes of rat brains.⁴⁷ It seems that PMAIP1 is highly regulated at the transcriptional and post-transcriptional levels.⁴⁸ In our study, a discrepancy between mRNA and protein levels for PMAIP1 was detected. This is in line with the post-translational modification and protein stability

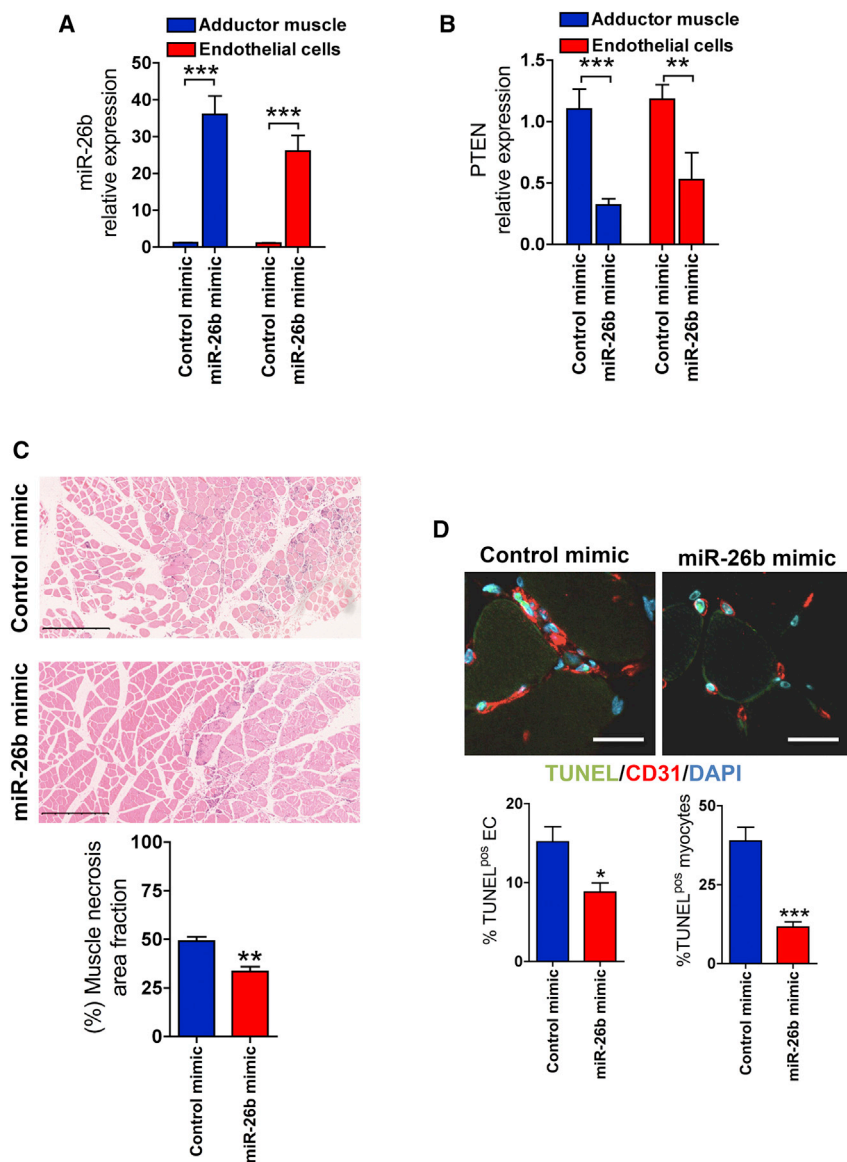


Figure 6. miR-26b Protects ECs and Myocytes from Ischemic Injury

(A and B) Expression of (A) miR-26b and (B) PTEN in ECs sorted from adductor muscles and total adductor muscles 3 days after ischemia and intramuscular oligonucleotide delivery. Error bars are mean \pm SEM; ** $p < 0.01$ compared to controls ($n = 5$ animals per group, unpaired t test). (C) Representative images of H&E staining of ischemic adductor muscles injected with miR-26b mimic or control mimic. Scale bar, 500 μm . Lower panel: quantitative analysis of muscle necrosis extent in the ischemic adductor muscles injected with miR-26b mimic and control mimic (necrosis area was normalized to the total muscle area) is shown ($n = 5$ per group). Error bars are mean \pm SEM; ** $p < 0.01$ compared to control mimic ($n = 5$ animals per group, unpaired t test). (D) Representative images of TUNEL staining of ischemic adductor muscles injected with miR-26b mimics or control mimic. CD31, red; TUNEL staining, green; DAPI, blue. Scale bars, 30 μm . Lower panel: quantification of ECs or myocytes positive for TUNEL staining is shown. Error bars are mean \pm SEM; * $p < 0.05$ and *** $p < 0.001$ compared to control ($n = 5$ animals per group, unpaired t test).

The inhibition of endogenous endothelial PTEN in cultured ECs potentially enhances a variety of VEGF-mediated cellular responses, including cell survival and migration.⁵¹ In agreement with our findings, PTEN has been previously characterized as a direct target of miR-26b in different cell types.^{37,52–54} Our study highlights that the survival effect of miR-26b on ECs is mediated mainly by regulating the expression of PTEN.

***In Vivo* Effects of miR-26b Overexpression**

In our study, the delivery of miR-26b mimics resulted in a high level of miR-26b expression in both animal models: Matrigel plug assay and limb ischemia. Moreover, the overexpression of miR-26b was associated with the inhibition of its identified target expression of PTEN. In agreement of *in vitro* functional assays, miR-26b overexpression enhances the microvascular growth and angiogenesis in the Matrigel plug model.

observed previously for this protein.^{49,50} The induction of a survival program by miR-26b could lead to an increase in the protein stability of cellular PMAIP1 without consequence on its pro-apoptotic activity. Therefore, it remains unclear whether the transcriptional downregulation of PMAIP1 by miR-26b is sufficient to contribute to its survival effect on ECs. PTEN possesses lipid phosphatase activity that functions as a direct antagonist of PI3K- and AKT1-dependent signaling. Notably, the PI3K-AKT1-mTOR pathway is involved in the regulation of constitutive PMAIP1 levels in cancer cells, and its inhibition has an impact on the accumulation of PMAIP1 protein.⁴⁹ With this in mind, the downregulation of PTEN due to miR-26b mimic and the consequent activation of the AKT1/mTOR pathway could be responsible for the accumulation of PMAIP1 in our experiments.

Interestingly, following ischemia injury, endogenous expression of the miR-26b level is decreased in the endothelium of skeletal muscles, while the forced local overexpression of miR-26b in the adductor muscles improves the survival of ECs and muscle fibers in the acute phase. In particular, miR-26b maintains an intact structure of the native capillary network, as revealed by the examination of the 3D structure of microvasculature. As a consequence of preserved native microvasculature network, it is expected that muscle fibers would be more tolerant to hypoxia and, thereby, exhibit less necrosis and inflammatory infiltrate.^{55,56} Nevertheless, we cannot exclude a direct effect of miR-26b mimic on the survival of muscle fibers following ischemic injury, since the overexpressed miR-26b was

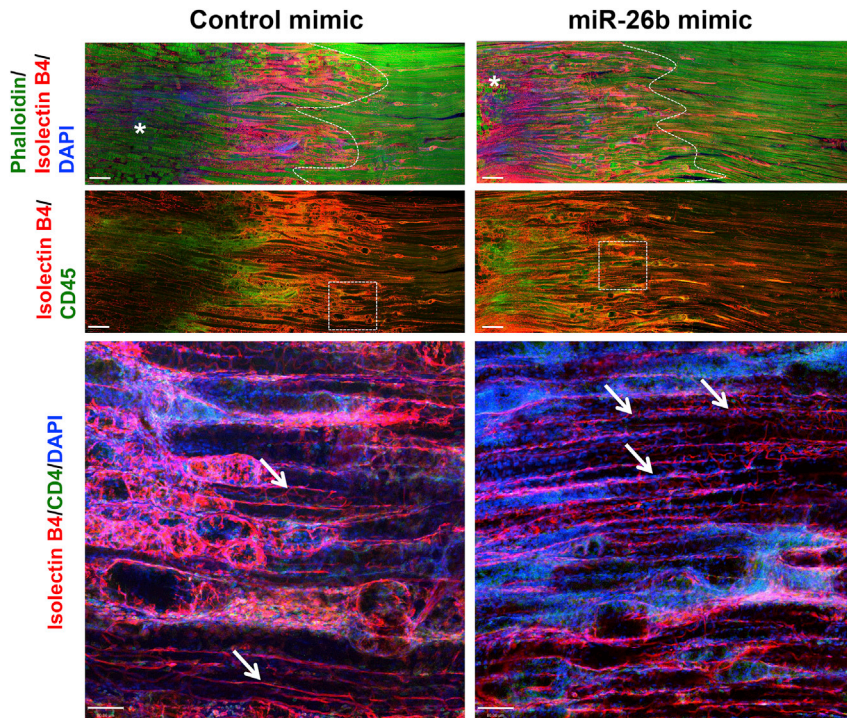


Figure 7. miR-26b Mimic Preserves the Native Microvasculature Network Morphology following Ischemia Injury

Representative confocal microscopy images of thick longitudinal sections for the ischemic adductor muscles injected with control mimic (left panels) or miR-26b mimic (right panels) at day 3 after ischemia. Upper panel: effect of exogenous miR-26b mimic injection on the survival of native muscle fibers and microvasculature network is shown. Asterisks denote the necrotic (dead) muscle fibers. Dotted line delimits the border of necrotic area. Myocytes (phalloidin, green), microvessels (isolectinB4, red), and nuclei (DAPI, blue) are shown. Scale bar, 340 μ m. Middle panel: effect of exogenous miR-26b mimic injection on the native microvasculature network and the infiltration of leukocytes in the ischemic muscles is shown. Leukocytes (CD45, green) and microvessels (isolectinB4, red) are shown. Scale bar, 340 μ m. Lower panel: inset of a higher magnification shows the microvascular network architecture in the necrotic area of ischemic adductor muscle. Arrowheads point to the preserved native microvasculature network in the necrotic areas. Leukocytes (CD45, green), microvessels (isolectinB4, red), and nuclei (DAPI, blue) are shown. Scale bar, 80 μ m.

detected in the muscle fraction. In our study, we found that a high level of miR-26b resulted in an inhibition of PTEN expression in the ischemic adductor muscles. At the molecular level, we can speculate that PI3K activation may occur via a loss of PTEN and, subsequently, blunt the adverse effect of ischemia on endothelium and muscle fibers.

Adductor muscles accommodate collateral vessels, which undergo a growth and remodeling process (arteriogenesis) to compensate for the lack of blood flow in the acute phase (2–7 days) after ischemia.⁵⁷ In our study, miR-26b overexpression in the adductor muscle did not affect the arteriogenesis, and no change in foot perfusion recovery was detectable using a laser speckle contrast imaging strategy. Further investigations are warranted to fully characterize the effect of miR-26b overexpression on angiogenesis and blood flow recovery in the chronic phase of limb ischemia.

Conclusions

High-content screening has been used as a functional discovery tool to identify the miRNAs related to cellular phenotypes.^{29,58} Gain-of-function genetic screens are well-established methods to identify genes sufficient to confer a particular cellular phenotype.⁵⁹ The use of a gain-of-function approach recapitulates the situation where the level of a particular miRNA is enhanced following the physiological or pathological stimulus. In our study, using this discovery tool, the role of miR-26b was highlighted in the EC growth, survival, and angiogenesis. Administration of miR-26b mimic could be a promising therapeutic approach for the ischemic vascular disease. Future pheno-

typic screenings of miRNA function using angiogenesis assays will likely reveal novel roles for miRNAs in vascular formation, function, and homeostasis.

MATERIALS AND METHODS

High-Content Screening of the miRNA Library

Pooled primary HUVECs were purchased from Lonza. Cells were maintained in EC medium (EGM-2, Lonza). HUVECs were reverse transfected in duplicate with a library of miRNA mimics (989 mature miRNAs with sense sequences, miRIDIAN microRNA Mimic Library, Dharmacon) in cell carrier 384-well flat clear-bottom black plates (PerkinElmer), using a standard reverse transfection protocol. Briefly, HUVECs (1,000 cells/well in 21 μ L complete EGM-2 media) were seeded into a well containing 14 μ L transfection mix (6.93 μ L Optimem, 0.07 μ L RNAi Max (Invitrogen), and 7 μ L 120 nM miRNA), giving a final mimic concentration of 24 nM. 24 hr later, cells were incubated with 35 μ L fresh EGM-2 media for an additional 48 hr at 37°C. At the 72-hr endpoint, cells were washed, fixed, and stained with DAPI dye. All liquid-handling steps, including seeding, fixation, washing, and staining, were performed using a Janus robotics (PerkinElmer). miR-503 mimic (inhibitor of EC growth)²¹ and non-targeting-control miRNA mimic were included with each screening plate as positive and negative controls, respectively.

Plates were imaged automatically at 10 \times magnification using the high-content imaging system (Operetta). Nine identically positioned fields were acquired from each well (covering the whole well area). Quantification of the cell number was performed automatically using

Harmony imaging analysis software. Positive and negative controls were served to measure Z' factor that reflects the quality of screen.⁶⁰ Cell number was normalized to non-targeting mimic miR-control of each plate to allow for the inter-plate comparisons. The data from replicates were then averaged and log₂ transformed to show the fold change. The selection cutoff for enhancer or inhibitor hits ($h_{e/i}$) was determined as follows,

$$h_{e/i} = \mu_{neg} \pm 10\sigma,$$

where μ_{neg} is the mean of negative controls (non-targeting control mimic and σ is the SD of the negative controls. The calculated cutoff for hit enhancer or inhibitor was equivalent to ± 1.8 -fold at linear scale and ± 0.85 at log₂ scale.

Cell Transfection and Transduction

Lipofectamine RNAiMAX (Thermo Fisher Scientific) was used to transfect HUVECs with miR-control mimic, miR-26b mimic, or anti-miR-26b (24 nM final concentration). Adenoviral particles of dominant-negative AKT1 (DN-AKT1) and EGFP (control vector) were produced and used as previously described.⁶¹

EdU Cell Proliferation Assay

DNA synthesis was assessed using Click-iT EdU Alexa Fluor 488 HCS kit (Thermo Fisher Scientific), according to the manufacturer's protocol. Briefly, EdU-labeling medium (10 μ M final concentration) was added to miRNA-transfected HUVEC culture and incubated for 6 hr before fixation. Next, the cultured cells were fixed with 4% paraformaldehyde and treated with 0.1% Triton X-100 for 15 min at room temperature. After washing with PBS, the samples were stained with Click-iT reaction cocktail working solution at room temperature for 30 min. The cells were stained with DAPI at room temperature for 20 min. The plates were imaged and quantified using high-content fluorescent microscopy (Operetta). The total cell number and percentage of EdU-positive cells were calculated from 9 fields/well using a 10 \times objective (Harmony software, PerkinElmer).

EC Migration Assay

Confluent HUVECs were transfected with controls or miR-26b mimic and plated on the ECIS chip array (8W1E) (Applied Biophysics). The migration speed was calculated in micrometers per hour as previously reported.⁶²

Caspase-3/7 Assay

Caspase-3/7 activity was measured using Caspase Glo 3/7 assay (Promega) according to the manufacturer's protocol.

Endothelial Tube Formation Assay

Matrigel (50 μ L/well) was added to the wells in a 96-well plate and allowed to polymerize at 37 °C for 30 min. HUVECs (15,000 cells) previously transfected with miR-26b mimic, anti-miR-26b, or miR-control mimic were added to the top of the Matrigel. After incubation for 8 hr, tube formation was assessed by high-content imaging using

the Operetta system. Total tube length and branching points were assessed by Metamorph image analysis software.⁶³

Bioinformatics for miR-26b Gene Target Prediction

Predicted miR-26b target-binding sites were obtained from TargetScan Human version (v.)7.0 (<http://www.targetscan.org>) and miRBase (<http://www.mirbase.org>). The prediction is based on scoring parameters such as context and conservation. Potential targets of miR-26b involved in cell growth- and survival-signaling pathways were identified using EnrichR online open source with Panther tool (<http://amp.pharm.mssm.edu/Enrichr/>).

siRNA Screening to Validate Predicted Gene Targets of miR-26b

HUVECs were reverse transfected in duplicate with a cherry-pick library of 48 siRNAs (OFF-Target Smartpool, Dharmacon) of predicted target gene candidates for miR-26b in 96-well plates. For cell growth assay, HUVECs were co-transfected with miR-26b or miR-control mimics after 24 hr. Cells were then incubated for an additional 72 hr. Next, cells were fixed and stained with DAPI. The plates were imaged and quantified using high-content fluorescent microscopy (Operetta). The total cell number was calculated from 9 fields/well using a 10 \times objective (Harmony software, PerkinElmer). Averaged cell count for each well (siRNA) was normalized to non-targeting siRNA and miR-control mimic well condition. For EC survival assay, after 48 hr of siRNA transfection, transfected HUVECs were exposed to H₂O₂ (500 μ M) for an additional 24 hr. Next, cells were fixed, stained, and imaged as described above. Averaged cell count for each well (siRNA) exposed to H₂O₂ was divided by the siRNA control condition (without H₂O₂ exposure). Then, values were multiplied by normalized cell count to non-targeting siRNA control. Both siRNA screens were performed in duplicate.

3' UTR Luciferase Assay

A luciferase assay was performed as previously described.²¹ Empty 3' UTR, PTEN 3' UTR, and PMAIP1 3' UTR vectors were from SwitchGear Genomic collection (Active Motif). We further validated the binding to PTEN and PMAIP1 using plasmids bearing the mutated version of the seed sequence in the 3' UTR. For PTEN, we deleted the first 4,000 bp of the 3' UTR sequence including the 4 binding sites. For PMAIP1, we mutated the single binding site in the 3' UTR (Figure S8). Mutations were introduced using GeneArt Site-Directed Mutagenesis System (Thermo Fisher Scientific). Primers for 3' UTR mutations were as follows: PTEN: forward 5'-ATGTGCAATAATGTAAAAATATGAAG-3', reverse 5'-GCACATTAGGACATGAGGGC-3'; and PMAIP1: forward 5'-TTACAAGAGTCTTATAACatataatTTTTTAGTTAA-3', reverse 5'-TTAACTAAAATATATATGTTATAAAGACTCTTGTA-3'. Luciferase constructs were co-transfected into HEK293T cells together with miR-26b mimic or miR-control mimic. p-SV-beta-Gal control vector was co-transfected in all conditions. Cells were cultured for 48 hr and assayed with the Luciferase and β -Galactosidase Reporter Assay Systems (Promega). Luciferase values were normalized to protein concentration and β -galactosidase activity.

qRT-PCR and miRNA Detection

Total RNA was extracted using mini RNeasy kits or miReasy kit (QIAGEN). For mRNA analysis, cDNA was amplified by real-time qPCR and normalized to 18S rRNA. Each reaction was performed in triplicate. Quantification was performed by the $2^{-\Delta\Delta C_t}$ method.⁶⁴ qPCR was used to measure PTEN, PMAIP1, PPP2R2A, and 18S rRNA. Primers were pre-designed from Sigma (KiCqStart Primers). Real-time quantification to measure miRNAs was performed with the TaqMan miRNA reverse transcription kit and miRNA assay (miR-26b) (Thermo Fisher Scientific) using Lightcycler 480 (Roche). miRNA expression was normalized to the U6 small nuclear RNA (snRU6).

Western Blotting

Cells were lysed with radioimmunoprecipitation assay (RIPA) buffer (Sigma) mixed with protease cocktail inhibitor and phosphatase inhibitors (Roche), and protein concentration was determined with a bicinchoninic acid (BCA) assay (Pierce). Equal amounts of protein per sample were separated by SDS-PAGE and transferred to an Immobilon-P polyvinylidene fluoride (PVDF) membrane (Millipore). Membranes were blocked with 5% skim milk, followed by incubation with primary antibodies β -actin (Sigma; 1:1,000), PMAIP1 (Cell Signaling Technology; 1:1,000), PTEN, (Cell Signaling Technology; 1:1,000), PPP2R2A (Cell Signaling Technology; 1:1,000), total AKT1 (Cell Signaling Technology; 1:1,000), and S473 p-AKT (Cell Signaling Technology; 1:1,000) at 4 °C overnight. Appropriate horseradish peroxidase (HRP)-conjugated secondary antibodies were incubated for 1 hr at room temperature (RT) before the detection of protein with enhanced chemoluminescence reagents (Millipore). Western blots were quantified using ImageJ software (NIH).

In Vivo Matrigel Plug Assay

Experiments involving mice were covered by project and personal licenses issued by the UK Home Office, and they were performed in accordance with the Guide for the Care and Use of Laboratory Animals (the Institute of Laboratory Animal Resources, 1996) and in accordance with Animal Research Report of *In vivo* Experiments (ARRIVE) guidelines. CD-1 mice (male, 10 weeks old) were subcutaneously injected into the groin regions of mice with 400 μ L Matrigel containing recombinant mouse basic FGF (bFGF) (PeproTech, 250 ng/mL) and heparin (Sigma, 50 U/mL) mixed with miR-mimic control or miR-26b mimics (lipids [Lipofectamine RNAiMAX reagent, ratio 1:1 in volume] 5 μ g/gel, n = 6 per group). After 12 days, mice were sacrificed, and the Matrigel plugs were removed and fixed in 4% paraformaldehyde. Paraffin cross-sections of plugs were deparaffinized and rehydrated. Antigen retrieval was performed by exposure to Proteinase K (Roche). The slides were blocked by incubating with 5% normal goat serum for 30 min, incubated with anti-CD31 primary antibody (Abcam; 1:200) overnight at 4 °C, and then incubated with Alexa 488-conjugated anti-rat immunoglobulin G (IgG) antibody (Thermo Fisher Scientific) and α -SM actin-cy3 (Sigma; 1:250) for 1 hr at room temperature. Sections were analyzed and photographed using a fluorescence microscope. CD31-positive neovessel area covered with α -SM actin inside plugs was quantified

using ImageJ software (NIH). Microvessel density was quantified in 25 fields/plug at each of three 1-mm-spaced sectioning planes of plugs. CD31-positive neovessel area was quantified using ImageJ software (NIH). Microvessel density is expressed per square micrometer.

Hindlimb Ischemia Model

Hindlimb ischemia was induced in mice as previously described.⁶⁵ Briefly, 12-week-old male CD-1 mice (Charles River Laboratories) were anesthetized with Isoflurane. The left femoral artery was ligated through a skin incision. The artery was then ligated to the external iliac artery at the distal point where it bifurcates into the saphenous and popliteal arteries. The femoral artery between two point ligations was then electro-coagulated. Mice were sacrificed and the adductor muscles were harvested for further analysis.

Isolation of Endothelial Cells from Mouse Limb Muscles

Ischemic and non-ischemic adductor muscles (n = 6 per group) were harvested at 3, 7, and 14 days after ischemia. Next, muscles were rinsed and digested with collagenase II (Worthington) plus DNase I (Sigma) using gentleMACS Dissociator, following the manufacturer's protocol. Next, ECs were immunomagnetic sorted using a CD31 and CD45 (Miltenyi Biotec) as previously reported.⁶⁶ RNA was extracted from EC fraction and muscle fraction for performing subsequent qPCR to measure the expression level of miR-26b, as described above. Purity of EC preparations was confirmed by flow cytometry using a cocktail of specific antibody markers for ECs: CD31 (Miltenyi Biotec; 1:50), CD144 (eBioscience; 1:50), and CD105 (eBioscience; 1:50).

Local Delivery of miRNA Mimics into Adductor Muscles

Of a mixture containing miR-26b mimic (1 μ g) or miR-control mimic (1 μ g), lipofectamine RNAiMAX reagent (Thermo Fisher Scientific, 10 μ L), and Opti-MEM (Thermo Fisher Scientific, 10 μ L), 20 μ L was injected into ischemic adductor muscles using a 0.3-mL insulin syringe with a 30G needle, as previously published.³³ At 3 days after surgery, mice were sacrificed, and the injected adductor muscles were harvested for further histology (n = 5 per group) or RNA analysis (n = 4 per group).

Laser Speckle Contrast Imaging of Blood Flow

Blood flow in the mouse paw was monitored using a Speckle Contrast Imager FLPI-2 (Moor Instruments, UK). The FLPI measurements were made in a warm (24 °C) and quiet environment. The charge-coupled device (CCD) camera was positioned 30 cm above the mouse paw. The contrast images were processed to produce a color-coded live flux image (red denoted high perfusion, blue signified low perfusion) using the moorFLPI-2 measurement module (Moor Instruments). Measurements were made in the paws area of non-ischemic and ischemic sides before and immediately after limb ischemia induction. Additional measurements were acquired 24, 48, and 72 hr after ischemia.

Histology, Immunostaining, and Morphometry

Ischemic adductor muscles were then removed and fixed with 4% buffered paraformaldehyde. Paraffin cross-sections were immunostained

for ECs using anti-CD31 antibodies as described above. TUNEL staining (Promega) was performed to detect apoptosis, according to the manufacturer's instructions. Next, the slides were co-stained with anti-CD31 for visualizing ECs, and the nuclei were further counterstained with DAPI (Thermo Fisher Scientific). We used the auto-fluorescent signal of myocytes with their distinct morphology to identify them in the tissue. The TUNEL-positive nuclei of ECs and myocytes were semi-quantified using NIH ImageJ software. The area of necrotic tissues in the adductor muscle was analyzed by H&E staining. Necrotic cells display a more glassy homogeneous appearance in the cytoplasm with increased eosinophilia, whereas the nuclear changes are reflected by karyolysis, pyknosis, and karyorrhexis. Necrotic area was defined as the percentage of area, which includes these necrotic myocytes, inflammatory cells, and interstitial cells, compared to the total muscle area. In analyzing arteriogenesis, sections were stained with anti-CD31 and anti- α -SM actin as described above. Tiled images of the entire adductor muscle were acquired at $\times 10$ for this analysis. The area of microvessels stained with α -SM actin, which were equal to or larger than 50 μm , were measured and normalized to the total adductor muscle area using ImageJ software (NIH).

Whole-Mount Immunohistochemistry

At 3 days post-ischemia, anesthetized mice were perfused and fixed under physiologic pressure with 4% paraformaldehyde. Adductor muscles were isolated, carefully dissected under stereomicroscope, and snap frozen. Samples were cut into slices of 150- μm thickness. Briefly, following incubation with blocking buffer, the samples were incubated with primary antibody rat anti-mouse CD45 (Pharmagen; 1:100) overnight at 4°C. Further incubation with the appropriate secondary antibody, alexa 488-conjugated Isolectin B4 (Invitrogen; 1:50), alexa 647-conjugated Phalloidin (Invitrogen; 1:100), and DAPI (Invitrogen), was performed. Whole-mount muscle imaging was done on an LSM 710 Zeiss confocal microscope. Maximum-projection confocal images of the adductor muscle microvasculature were generated from z stacks (30–70 μm , 1- to 10- μm step size depending on specimen size, staining, and objective used) acquired starting at the medial surface of the adductor muscle specimens. To visualize large areas of the microvasculature network on the confocal microscope, a tile-scanning technique was employed whereby multiple overlapping (10% overlap) maximum-projection images were acquired with a 10 \times or 20 \times objective and a composite image was constructed by arraying the individual images using ZEN software (Zeiss).

Statistical Analysis

Screen data were visualized using TIBCO Spotfire analytic software (PerkinElmer). Comparisons between different conditions were assessed using 2-tailed Student's t test. Differences among groups were elicited using ANOVA statistical test followed by Bonferroni post hoc analyses as appropriate. Continuous data are expressed as mean \pm SEM; a p value < 0.05 was considered statistically significant. Statistical analyses and graphics were performed using GraphPad Prism v.5.0.

SUPPLEMENTAL INFORMATION

Supplemental Information includes eight figures and can be found with this article online at <https://doi.org/10.1016/j.omtn.2018.08.006>.

AUTHOR CONTRIBUTIONS

A.M., D.M., A.C., and A.A. designed and conducted the *in vitro* experiments. M.M. and A.A. designed and conducted the *in vivo* experiments. A.H., D.E., and A.A. conducted the high-throughput screening. A.C. and A.A. directed the research and participated in the design and interpretation of experiments and the writing of the manuscript.

CONFLICTS OF INTEREST

The authors declare no conflicts of interest.

ACKNOWLEDGMENTS

A.A. is supported by the intermediate fellowship awarded by the Oxford BHF Centre of Research Excellence (RE/08/004/23915). This study was funded by the Oxford BHF Centre of Research Excellence (RE/08/004 and RE/13/1/30181) and a BHF Project grant (PG/16/58/32275). A.M. is supported by the Wellcome-University of Edinburgh Institutional Strategic Support Fund (ISSF3).

REFERENCES

- Adams, R.H., and Alitalo, K. (2007). Molecular regulation of angiogenesis and lymphangiogenesis. *Nat. Rev. Mol. Cell Biol.* 8, 464–478.
- Potente, M., Gerhardt, H., and Carmeliet, P. (2011). Basic and therapeutic aspects of angiogenesis. *Cell* 146, 873–887.
- Mentzer, S.J., and Konerding, M.A. (2014). Intussusceptive angiogenesis: expansion and remodeling of microvascular networks. *Angiogenesis* 17, 499–509.
- Chavakis, E., and Dimmeler, S. (2002). Regulation of endothelial cell survival and apoptosis during angiogenesis. *Arterioscler. Thromb. Vasc. Biol.* 22, 887–893.
- Potente, M., Urbich, C., Sasaki, K., Hofmann, W.K., Heeschen, C., Aicher, A., Kollipara, R., DePinho, R.A., Zeiher, A.M., and Dimmeler, S. (2005). Involvement of Foxo transcription factors in angiogenesis and postnatal neovascularization. *J. Clin. Invest.* 115, 2382–2392.
- Fujio, Y., and Walsh, K. (1999). Akt mediates cytoprotection of endothelial cells by vascular endothelial growth factor in an anchorage-dependent manner. *J. Biol. Chem.* 274, 16349–16354.
- Karar, J., and Maity, A. (2011). Pi3k/akt/mtor pathway in angiogenesis. *Front. Mol. Neurosci.* 4, 51.
- Fulton, D., Gratton, J.P., McCabe, T.J., Fontana, J., Fujio, Y., Walsh, K., Franke, T.F., Papapetropoulos, A., and Sessa, W.C. (1999). Regulation of endothelium-derived nitric oxide production by the protein kinase Akt. *Nature* 399, 597–601.
- Jiang, B.H., Zheng, J.Z., Aoki, M., and Vogt, P.K. (2000). Phosphatidylinositol 3-kinase signaling mediates angiogenesis and expression of vascular endothelial growth factor in endothelial cells. *Proc. Natl. Acad. Sci. USA* 97, 1749–1753.
- Lelievre, E., Bourbon, P.M., Duan, L.J., Nussbaum, R.L., and Fong, G.H. (2005). Deficiency in the p110alpha subunit of PI3K results in diminished Tie2 expression and Tie2(-/-)-like vascular defects in mice. *Blood* 105, 3935–3938.
- Carmeliet, P., Lampugnani, M.G., Moons, L., Breviaro, F., Compernelle, V., Bono, F., Balconi, G., Spagnuolo, R., Oosthuysen, B., Dewerchin, M., et al. (1999). Targeted deficiency or cytosolic truncation of the VE-cadherin gene in mice impairs VEGF-mediated endothelial survival and angiogenesis. *Cell* 98, 147–157.
- Ackah, E., Yu, J., Zoellner, S., Iwakiri, Y., Skurk, C., Shibata, R., Ouchi, N., Easton, R.M., Galasso, G., Birnbaum, M.J., et al. (2005). Akt1/protein kinase Balpha is critical for ischemic and VEGF-mediated angiogenesis. *J. Clin. Invest.* 115, 2119–2127.

13. Duscha, B.D., Robbins, J.L., Jones, W.S., Kraus, W.E., Lye, R.J., Sanders, J.M., Allen, J.D., Regensteiner, J.G., Hiatt, W.R., and Annex, B.H. (2011). Angiogenesis in skeletal muscle precede improvements in peak oxygen uptake in peripheral artery disease patients. *Arterioscler. Thromb. Vasc. Biol.* *31*, 2742–2748.
14. Bartel, D.P. (2009). MicroRNAs: target recognition and regulatory functions. *Cell* *136*, 215–233.
15. Zhang, R., and Su, B. (2009). Small but influential: the role of microRNAs on gene regulatory network and 3'UTR evolution. *J. Genet. Genomics* *36*, 1–6.
16. Yang, W.J., Yang, D.D., Na, S., Sandusky, G.E., Zhang, Q., and Zhao, G. (2005). Dicer is required for embryonic angiogenesis during mouse development. *J. Biol. Chem.* *280*, 9330–9335.
17. Suárez, Y., Fernández-Hernando, C., Yu, J., Gerber, S.A., Harrison, K.D., Pober, J.S., Trueta-Arispe, M.L., Merckenschlager, M., and Sessa, W.C. (2008). Dicer-dependent endothelial microRNAs are necessary for postnatal angiogenesis. *Proc. Natl. Acad. Sci. USA* *105*, 14082–14087.
18. Kuehbachner, A., Urbich, C., Zeiher, A.M., and Dimmeler, S. (2007). Role of Dicer and Drosha for endothelial microRNA expression and angiogenesis. *Circ. Res.* *101*, 59–68.
19. Nicoli, S., Knyphausen, C.P., Zhu, L.J., Lakshmanan, A., and Lawson, N.D. (2012). miR-221 is required for endothelial tip cell behaviors during vascular development. *Dev. Cell* *22*, 418–429.
20. Yin, K.J., Olsen, K., Hamblin, M., Zhang, J., Schwendeman, S.P., and Chen, Y.E. (2012). Vascular endothelial cell-specific microRNA-15a inhibits angiogenesis in hindlimb ischemia. *J. Biol. Chem.* *287*, 27055–27064.
21. Caporali, A., Meloni, M., Völlenkle, C., Bonci, D., Sala-Newby, G.B., Addis, R., Spinetti, G., Losa, S., Masson, R., Baker, A.H., et al. (2011). Deregulation of microRNA-503 contributes to diabetes mellitus-induced impairment of endothelial function and reparative angiogenesis after limb ischemia. *Circulation* *123*, 282–291.
22. Caporali, A., Meloni, M., Nailor, A., Mitić, T., Shantikumar, S., Riu, F., Sala-Newby, G.B., Rose, L., Besnier, M., Katare, R., et al. (2015). p75(NTR)-dependent activation of NF- κ B regulates microRNA-503 transcription and pericyte-endothelial crosstalk in diabetes after limb ischaemia. *Nat. Commun.* *6*, 8024.
23. Stather, P.W., Sylvius, N., Wild, J.B., Choke, E., Sayers, R.D., and Bown, M.J. (2013). Differential microRNA expression profiles in peripheral arterial disease. *Circ Cardiovasc Genet* *6*, 490–497.
24. Fichtlscherer, S., De Rosa, S., Fox, H., Schwietz, T., Fischer, A., Liebetrau, C., Weber, M., Hamm, C.W., Röxe, T., Müller-Ardogan, M., et al. (2010). Circulating microRNAs in patients with coronary artery disease. *Circ. Res.* *107*, 677–684.
25. Chen, W., and Li, S. (2017). Circulating microRNA as a novel biomarker for pulmonary arterial hypertension due to congenital heart disease. *Pediatr. Cardiol.* *38*, 86–94.
26. Björklund, M., Taipale, M., Varjosalo, M., Saharinen, J., Lahdenperä, J., and Taipale, J. (2006). Identification of pathways regulating cell size and cell-cycle progression by RNAi. *Nature* *439*, 1009–1013.
27. Zhang, H., Hao, Y., Yang, J., Zhou, Y., Li, J., Yin, S., Sun, C., Ma, M., Huang, Y., and Xi, J.J. (2011). Genome-wide functional screening of miR-23b as a pleiotropic modulator suppressing cancer metastasis. *Nat. Commun.* *2*, 554.
28. Jentsch, C., Leierseder, S., Loyer, X., Flohrschütz, I., Sassi, Y., Hartmann, D., Thum, T., Laggerbauer, B., and Engelhardt, S. (2012). A phenotypic screen to identify hypertrophy-modulating microRNAs in primary cardiomyocytes. *J. Mol. Cell. Cardiol.* *52*, 13–20.
29. Eulalio, A., Mano, M., Dal Ferro, M., Zentilin, L., Sinagra, G., Zacchigna, S., and Giacca, M. (2012). Functional screening identifies miRNAs inducing cardiac regeneration. *Nature* *492*, 376–381.
30. Wahlquist, C., Jeong, D., Rojas-Muñoz, A., Kho, C., Lee, A., Mitsuyama, S., van Mil, A., Park, W.J., Sluijter, J.P., Doevendans, P.A., et al. (2014). Inhibition of miR-25 improves cardiac contractility in the failing heart. *Nature* *508*, 531–535.
31. Sun, H., Lesche, R., Li, D.M., Liliental, J., Zhang, H., Gao, J., Gavrilova, N., Mueller, B., Liu, X., and Wu, H. (1999). PTEN modulates cell cycle progression and cell survival by regulating phosphatidylinositol 3,4,5-trisphosphate and Akt/protein kinase B signaling pathway. *Proc. Natl. Acad. Sci. USA* *96*, 6199–6204.
32. Yakovlev, A.G., Di Giovanni, S., Wang, G., Liu, W., Stoica, B., and Faden, A.I. (2004). BOK and NOXA are essential mediators of p53-dependent apoptosis. *J. Biol. Chem.* *279*, 28367–28374.
33. Lesizza, P., Prosdocimo, G., Martinelli, V., Sinagra, G., Zacchigna, S., and Giacca, M. (2017). Single-dose intracardiac injection of pro-regenerative microRNAs improves cardiac function after myocardial infarction. *Circ. Res.* *120*, 1298–1304.
34. Chamorro-Jorganes, A., Lee, M.Y., Araldi, E., Landskroner-Eiger, S., Fernández-Fuertes, M., Sahraei, M., Quiles Del Rey, M., van Solingen, C., Yu, J., Fernández-Hernando, C., et al. (2016). Vegf-induced expression of mir-17-92 cluster in endothelial cells is mediated by erk/elk1 activation and regulates angiogenesis. *Circ. Res.* *118*, 38–47.
35. Spinetti, G., Fortunato, O., Caporali, A., Shantikumar, S., Marchetti, M., Meloni, M., Descamps, B., Floris, I., Sangalli, E., Vono, R., et al. (2013). MicroRNA-15a and microRNA-16 impair human circulating proangiogenic cell functions and are increased in the proangiogenic cells and serum of patients with critical limb ischemia. *Circ. Res.* *112*, 335–346.
36. Fiedler, J., Jazbutyte, V., Kirchmaier, B.C., Gupta, S.K., Lorenzen, J., Hartmann, D., Galuppo, P., Kneitz, S., Pena, J.T., Sohn-Lee, C., et al. (2011). MicroRNA-24 regulates vascularility after myocardial infarction. *Circulation* *124*, 720–730.
37. Huse, J.T., Brennan, C., Hambardzumyan, D., Wee, B., Pena, J., Rouhanifard, S.H., Sohn-Lee, C., le Sage, C., Agami, R., Tuschl, T., and Holland, E.C. (2009). The PTEN-regulating microRNA miR-26a is amplified in high-grade glioma and facilitates gliomagenesis in vivo. *Genes Dev.* *23*, 1327–1337.
38. Icli, B., Wara, A.K., Moselehi, J., Sun, X., Plovie, E., Cahill, M., Marchini, J.F., Schissler, A., Padera, R.F., Shi, J., et al. (2013). MicroRNA-26a regulates pathological and physiological angiogenesis by targeting BMP/SMAD1 signaling. *Circ. Res.* *113*, 1231–1241.
39. Leeper, N.J., Raiesdana, A., Kojima, Y., Chun, H.J., Azuma, J., Maegdefessel, L., Kundu, R.K., Quertermous, T., Tsao, P.S., and Spin, J.M. (2011). MicroRNA-26a is a novel regulator of vascular smooth muscle cell function. *J. Cell. Physiol.* *226*, 1035–1043.
40. Ji, J., Shi, J., Budhu, A., Yu, Z., Forgues, M., Roessler, S., Ambs, S., Chen, Y., Meltzer, P.S., Croce, C.M., et al. (2009). MicroRNA expression, survival, and response to interferon in liver cancer. *N. Engl. J. Med.* *361*, 1437–1447.
41. Liu, X.X., Li, X.J., Zhang, B., Liang, Y.J., Zhou, C.X., Cao, D.X., He, M., Chen, G.Q., He, J.R., and Zhao, Q. (2011). MicroRNA-26b is underexpressed in human breast cancer and induces cell apoptosis by targeting SLC7A11. *FEBS Lett.* *585*, 1363–1367.
42. Pan, C., Yan, X., Li, H., Huang, L., Yin, M., Yang, Y., Gao, R., Hong, L., Ma, Y., Shi, C., et al. (2017). Systematic literature review and clinical validation of circulating microRNAs as diagnostic biomarkers for colorectal cancer. *Oncotarget* *8*, 68317–68328.
43. Lin, J., Zhang, L., Huang, H., Huang, Y., Huang, L., Wang, J., Huang, S., He, L., Zhou, Y., Jia, W., et al. (2015). MiR-26b/KPNA2 axis inhibits epithelial ovarian carcinoma proliferation and metastasis through downregulating OCT4. *Oncotarget* *6*, 23793–23806.
44. Duan, G., Ren, C., Zhang, Y., and Feng, S. (2015). MicroRNA-26b inhibits metastasis of osteosarcoma via targeting CTGF and Smad1. *Tumour Biol.* *36*, 6201–6209.
45. Xia, M., Duan, M.L., Tong, J.H., and Xu, J.G. (2015). MiR-26b suppresses tumor cell proliferation, migration and invasion by directly targeting COX-2 in lung cancer. *Eur. Rev. Med. Pharmacol. Sci.* *19*, 4728–4737.
46. Czabotar, P.E., Lee, E.F., van Delft, M.F., Day, C.L., Smith, B.J., Huang, D.C., Fairlie, W.D., Hinds, M.G., and Colman, P.M. (2007). Structural insights into the degradation of Mcl-1 induced by BH3 domains. *Proc. Natl. Acad. Sci. USA* *104*, 6217–6222.
47. Kim, J.Y., Ahn, H.J., Ryu, J.H., Suk, K., and Park, J.H. (2004). BH3-only protein Noxa is a mediator of hypoxic cell death induced by hypoxia-inducible factor 1 α . *J. Exp. Med.* *199*, 113–124.
48. Ploner, C., Kofler, R., and Villunger, A. (2008). Noxa: at the tip of the balance between life and death. *Oncogene* *27* (Suppl 1), S84–S92.
49. Dengler, M.A., Weilbacher, A., Gutekunst, M., Staiger, A.M., Vöhringer, M.C., Horn, H., Ott, G., Aulitzky, W.E., and van der Kuip, H. (2014). Discrepant NOXA (PMAIP1) transcript and NOXA protein levels: a potential Achilles' heel in mantle cell lymphoma. *Cell Death Dis.* *5*, e1013.
50. Pang, X., Zhang, J., Lopez, H., Wang, Y., Li, W., O'Neill, K.L., Evans, J.J., George, N.M., Long, J., Chen, Y., and Luo, X. (2014). The carboxyl-terminal tail of Noxa protein regulates the stability of Noxa and Mcl-1. *J. Biol. Chem.* *289*, 17802–17811.

51. Huang, J., and Kontos, C.D. (2002). PTEN modulates vascular endothelial growth factor-mediated signaling and angiogenic effects. *J. Biol. Chem.* *277*, 10760–10766.
52. Zhang, L., Huang, C., Guo, Y., Gou, X., Hinsdale, M., Lloyd, P., and Liu, L. (2015). MicroRNA-26b modulates the NF- κ B pathway in alveolar macrophages by regulating PTEN. *J. Immunol.* *195*, 5404–5414.
53. Palumbo, T., Faucz, F.R., Azevedo, M., Xekouki, P., Iliopoulos, D., and Stratakis, C.A. (2013). Functional screen analysis reveals miR-26b and miR-128 as central regulators of pituitary somatomammotrophic tumor growth through activation of the PTEN-AKT pathway. *Oncogene* *32*, 1651–1659.
54. Li, G., Ning, C., Ma, Y., Jin, L., Tang, Q., Li, X., Li, M., and Liu, H. (2017). Mir-26b promotes 3t3-l1 adipocyte differentiation through targeting pten. *DNA Cell Biol.* *36*, 672–681.
55. Hudlicka, O. (2011). Microcirculation in skeletal muscle. *Muscles Ligaments Tendons J.* *1*, 3–11.
56. Eltzschig, H.K., and Eckle, T. (2011). Ischemia and reperfusion—from mechanism to translation. *Nat. Med.* *17*, 1391–1401.
57. Faber, J.E., Chilian, W.M., Deindl, E., van Royen, N., and Simons, M. (2014). A brief etymology of the collateral circulation. *Arterioscler. Thromb. Vasc. Biol.* *34*, 1854–1859.
58. Zhao, Z., Ma, X., Hsiao, T.H., Lin, G., Kosti, A., Yu, X., Suresh, U., Chen, Y., Tomlinson, G.E., Pertselmidis, A., and Du, L. (2014). A high-content morphological screen identifies novel microRNAs that regulate neuroblastoma cell differentiation. *Oncotarget* *5*, 2499–2512.
59. Pritsker, M., Ford, N.R., Jenq, H.T., and Lemischka, I.R. (2006). Genomewide gain-of-function genetic screen identifies functionally active genes in mouse embryonic stem cells. *Proc. Natl. Acad. Sci. USA* *103*, 6946–6951.
60. Zhang, J.H., Chung, T.D., and Oldenburg, K.R. (1999). A simple statistical parameter for use in evaluation and validation of high throughput screening assays. *J. Biomol. Screen.* *4*, 67–73.
61. Caporali, A., and Emanuelli, C. (2011). MicroRNA regulation in angiogenesis. *Vascul. Pharmacol.* *55*, 79–86.
62. Giaever, I., and Keese, C.R. (1991). Micromotion of mammalian cells measured electrically. *Proc. Natl. Acad. Sci. USA* *88*, 7896–7900.
63. Al Haj Zen, A., Nawrot, D.A., Howarth, A., Caporali, A., Ebner, D., Vernet, A., Schneider, J.E., and Bhattacharya, S. (2016). The retinoid agonist tazarotene promotes angiogenesis and wound healing. *Mol. Ther.* *24*, 1745–1759.
64. Schmittgen, T.D., and Livak, K.J. (2008). Analyzing real-time PCR data by the comparative C(T) method. *Nat. Protoc.* *3*, 1101–1108.
65. Madeddu, P., Emanuelli, C., Pelosi, E., Salis, M.B., Cerio, A.M., Bonanno, G., Patti, M., Stassi, G., Condorelli, G., and Peschle, C. (2004). Transplantation of low dose CD34+KDR+ cells promotes vascular and muscular regeneration in ischemic limbs. *FASEB J.* *18*, 1737–1739.
66. Larsson, E., Fredlund Fuchs, P., Heldin, J., Barkefors, I., Bondjers, C., Genové, G., Arrondel, C., Gerwins, P., Kurschat, C., Schermer, B., et al. (2009). Discovery of microvascular miRNAs using public gene expression data: miR-145 is expressed in pericytes and is a regulator of Fli1. *Genome Med.* *1*, 108.

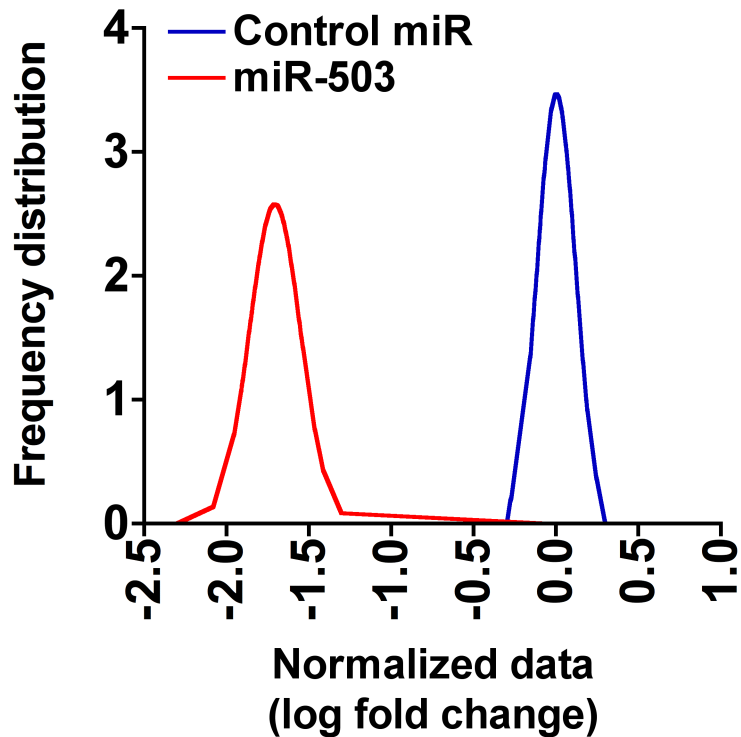
OMTN, Volume 13

Supplemental Information

**Phenotypic miRNA Screen Identifies miR-26b
to Promote the Growth and Survival
of Endothelial Cells**

Andrea Martello, David Mellis, Marco Meloni, Alison Howarth, Daniel Ebner, Andrea Caporali, and Ayman Al Haj Zen

A)



B)

<i>Plate</i>	<i>Replicate</i>	<i>Z' factor</i>
1	1	0.5
1	2	0.3
2	1	0.4
2	2	0.7
3	1	0.6
3	2	0.4
4	1	0.3
4	2	0.3

Figure S1. Control performance and plate QC. **A)** Graph showing the separation between the distributions of the positive (miR-503 mimic) and negative controls (miR control mimic) in the primary screen. **B)** Plate performance in the primary phenotypic screen was assessed by standard Z' factor was calculated for each screen plate using the positive and negative controls integrated into the same plate. All plates were passed (Z' factor ≥ 0.3).

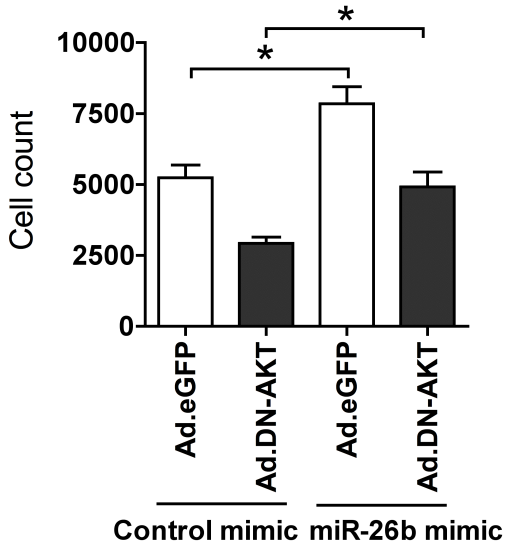
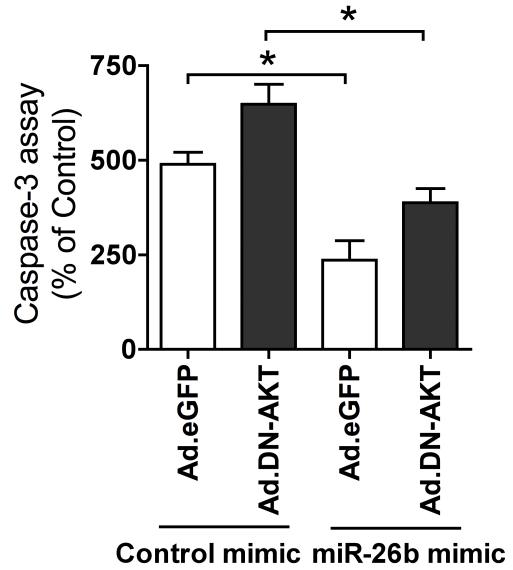
A)**B)**

Figure S2. The proliferative and survival effect of miR-26b is mediated by AKT signaling. Effect of miR-26b mimics on cell proliferation assessed by cell count (**A**) and on apoptosis measured by caspase-3 activity (**B**) with adenovirus mediated transfer of dominant negative inhibitors of AKT (Ad.DN.AKT) or with GFP vector control (Ad.eGFP). Cells were analyzed 72 hours following miRNA mimic transfection. Error bars, mean \pm s.e.m., *P<0.05, (n=4 replicates derived from 3 independent experiments, unpaired t-test)

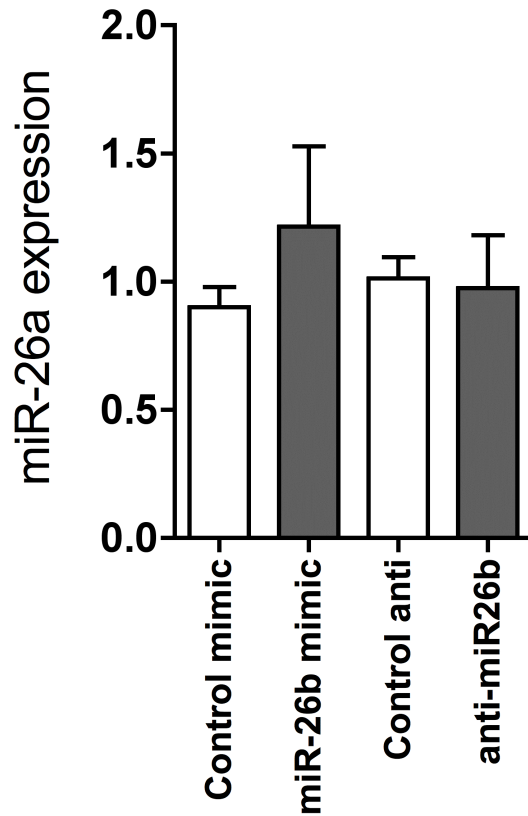


Figure S3. Effect of miR-26b overexpression and inhibition on endogenous miR-26a expression in HUVEC. RNA was isolated for performing RT-qPCR after 72 hours of transfection. miR-26b levels were normalized against snRU6 control. Error bars, mean±SEM (n=6 replicates).

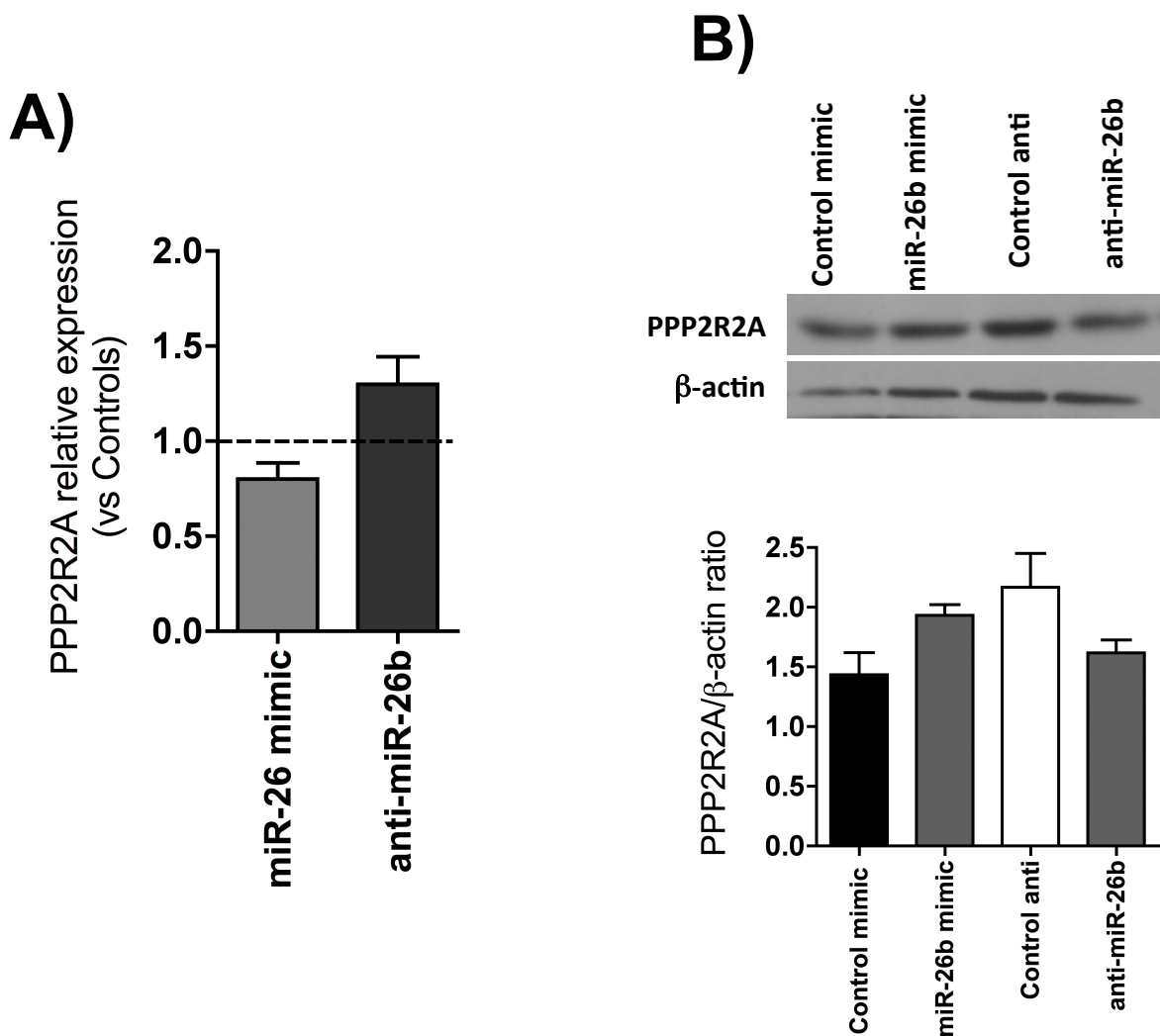


Figure S4. Validation assays for the PPP2R2A hit target of miR-26b **A)** HUVEC were transfected with miR-26b mimic, anti-miR-26b, miR-control mimic or anti-miR control. Three days post transfection, RNA was extracted and the levels of PPP2R2A was determined by qRT-PCR. Values were normalized to S18 and then to the controls (mimic or anti-miR). Data are shown as the mean \pm SEM of 4 replicates. **B)** Transfected HUVEC with different vectors were lysed and the protein expression of PPP2R2A was analyzed by immunoblotting. β -actin was detected as a loading control. *Lower Panel:* graph represents the quantitative data of Error bars, mean \pm s.e.m. (n=3 replicates).

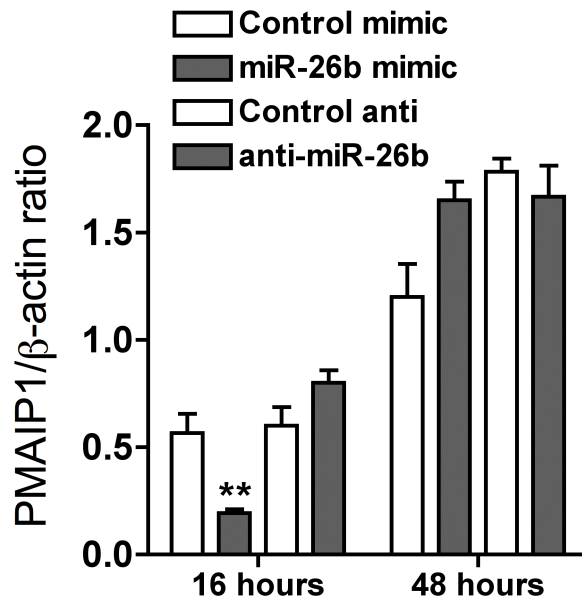
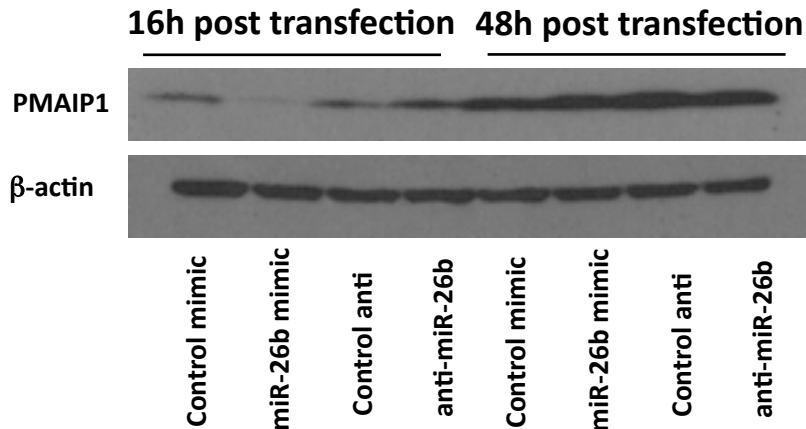


Figure S5. Time course of PMAIP1 protein expression following miR-26b overexpression or inhibition. HUVEC were transfected with miR-26b mimic, anti-miR-26b, miR-control mimic or anti-miR control. 16 hours or 28 hours post transfection, HUVEC were lysed and the protein expression of PMAIP1 was analyzed by immunoblotting. β -actin was detected as a loading control. Lower Panel: graph represents the quantitative data of. Error bars, mean \pm s.e.m., (** $P < 0.01$, ($n = 3$ replicates, unpaired t-test)

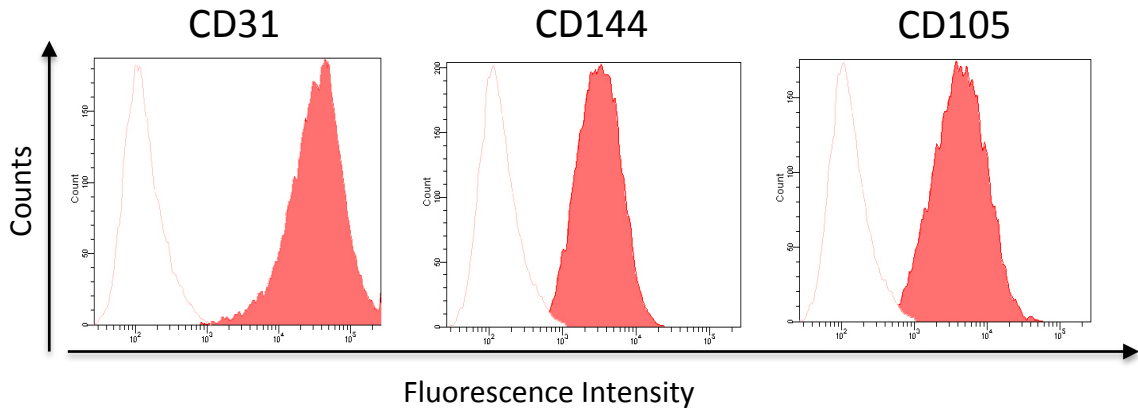


Figure S6. The expression profile of specific endothelium markers on endothelial cells (CD31^{pos}/CD45^{neg}) sorted cells from the adductor muscles using MACS[®] microbead system, were analyzed by Flow Cytometry. *Empty histograms* represents purified endothelial cells without primary antibody; *Filled histograms* represent the purified endothelial cells incubated with anti-CD31 (pecam1), anti-CD144 (ve-cadherin) and anti-CD105 (endoglin) antibodies.

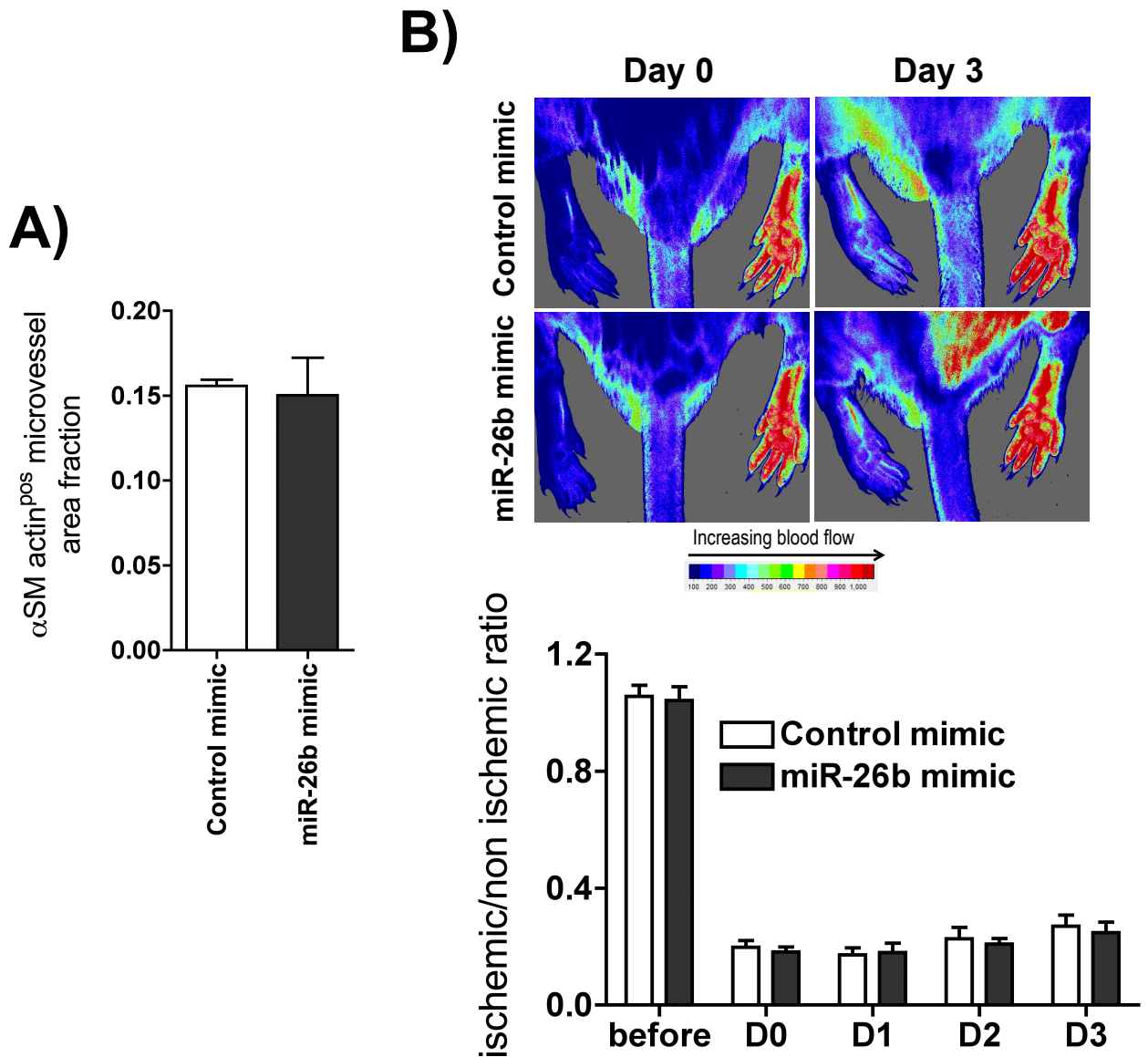


Figure S7. Effect of local miR-26b overexpression in the adductor muscle on the distal blood flow recovery in the paws and on arteriogenesis. Limb ischemia was induced by left femoral artery excision. At same occasion, miR-26b mimic or control mimic was locally injected in the adductor muscle. **A)** The area of microvessels stained with α -SM (smooth muscle) actin, which are equal or larger than $50\mu\text{m}$ were measured and normalized to the total adductor muscle area. The quantification was carried on cross-sections of ischemic adductor muscles treated with control mimic or miR-26b mimic at day 3 after ischemia injury. Data are presented as mean \pm SEM. (n=4 per group). **B)** Laser speckle contrast imaging was applied to measure the tissue perfusion in paws of contralateral non-ischemic limb and ischemic limb. *Lower panel*; Quantitative analysis of laser speckle contrast perfusion imaging before, immediately after the surgery and at the 1, 2, and 3 day time point presented as perfusion ratios (ischemic/non-ischemic side) in the paws. Data are presented as mean \pm SEM. (n=5 per group).

